Characterization of the Optical Properties of Metalloporphyrins in TiO_2 Sol-gel Films for Photon Upconversion Applications

A Thesis Submitted

to the College of Graduate Studies and Research

in Partial Fulfillment of the Requirements

for the Degree of Master of Science

in the Department of Chemistry

University of Saskatchewan

by

Terri Thunder

Department of Chemistry

University of Saskatchewan

PERMISSION TO USE

In presenting this thesis in partial fulfillment of the requirements for a postgraduate degree from the University of Saskatchewan, it is agreed that the Libraries of this University may make it freely available for inspection. Permission for copying of this thesis in any manner, in whole or in part, for scholarly purposes may be granted by the professors who supervised this thesis work or, in their absence, by the Head of the Department of Chemistry or the Dean of the College of Graduate Studies and Research at the University of Saskatchewan. Any copying, publication, or use of this thesis, or parts thereof, for financial gain without the written permission of the author is strictly prohibited. Proper recognition shall be given to the author and to the University of Saskatchewan in any scholarly use which may be made of any material in this thesis.

Requests for permission to copy or to make other use of material in this thesis in whole or part should be addressed to:

Head of the Department of Chemistry

University of Saskatchewan

110 Science Place

Saskatoon, Saskatchewan S7N 5C9

ABSTRACT

The photophysical properties of a series of Zn (II) porphyrins adsorbed onto a semiconductor were investigated using steady-state absorbance and emission measurements. The ability of the porphyrins to undergo triplet-triplet annihilation (TTA), a photophysical process through which photons in the red and near-infrared (NIR) regions of the optical spectrum can be converted into higher energy photons (upconversion), was explored. Aggregation capabilities were determined to verify possibility of these molecules to undergo triplet-triplet annihilation (TTA). TTA has significant potential for increasing the efficiency of dye-sensitized solar cells (DSSCs) by upconverting photons in the energy rich NIR region of the solar spectrum. A key requirement for efficient TTA is aggregation of the sensitizer dye, and in this thesis, we have examined the aggregation of porphyrins in TiO_2-based sol-gel films. Solution phase absorption and emission studies were conducted using zinc (II) tetraphenylporphyrin and three of its functionalized derivatives, tetra(4-aminophenyl)porphyrin Zn(II), tetra(4-carboxyphenyl)porphyrin Zn(II), and tetra(4-sulfonatophenyl)porphyrin Zn(II), to evaluate their potential as DSSC sensitizers on TiO_2 thin films. Mesoporous TiO_2 thin films were synthesized, using a polymer-templating sol-gel route, and characterized with tunneling electron microscopy (TEM), atomic force microscopy (AFM), and UV-Vis absorbance measurements. Spectroscopy measurements were also carried out on porphyrin-sensitized TiO_2 thin films and compared to solution-based results. A simple DSSC was constructed and used to further explore the application of zinc (II) porphyrin sensitizers in photovoltaic applications.

ACKNOWLEDGEMENTS

I would first like to thank my supervisor, Matthew Paige, for giving me the opportunity to work in his lab. He took a chance on me that I'm sure not many would have, and for that I am extremely grateful. His patience and guidance made my time spent in his lab memorable.

I would like to thank Ron Steer for allowing me to crash in on his group meetings and consult with him when I needed clarification and guidance. His excitement when talking about research was always inspiring. Thanks to Rob Scott for his help on the materials portion of this project and for letting me use his furnace. I would also like to thank Tesfalidet Balcha for his help on characterizing the TiO_2. I would like to thank my committee member, Andrew Grosvenor, for his input on this project, and for allowing me to use his furnaces.

Thanks to my group members, members of other groups and University staff for their help, especially Sunish, Brook, and Mike. I would like to thank Yin Lu for her help when I first started this program. I thank Conie for how much she has helped me with everything. I am grateful for her support, guidance, advice, and above all, her friendship. My thanks are extended to Michelle for offering support when I needed it, and of course, for the countless Xbox gaming sessions. Also, thanks to Louis and Myron for the supper and coffee visits.

I would also like to thank the Department of Chemistry at the University of Saskatchewan and Thunderchild First Nation for their financial support.

Finally, I would like to thank my family and friends for their support and encouragement. Special thanks to Sarah Kinzel for being there for me.

Dedicated to my parents,

Cheryl & Steven Thunder

Table of Contents

List of Tables

List of Figures

List of Abbreviations

AFM	atomic force microscopy
AM	air mass
DSSC	dye-sensitized solar cells
FF	fill factor
FTO	fluorine-doped tin oxide
FWHM	full-width half maxima
HOMO	highest occupied molecular orbital
I-V	current-voltage
IC	internal conversion
I_{max}	maximum current
IPCE	incident photon-to-current conversion efficiency
ISC	intersystem crossing
J_{max}	maximum current density
J_{sc}	short-circuit photocurrent density
LMCT	ligand-to-metal charge transfer
LUMO	lowest unoccupied molecular orbital
MLCT	metal-to-ligand charge transfer
NIR	near-infrared
OEP	octaethylporphyrin
P123	poly(ethylene glycol)-block-poly(propylene glycol)-block-poly(ethylene glycol)
P_{in}	intensity of the incident light
P_{max}	maximum power of the solar cell

PMMA	poly(methyl methacrylate)
S_0	ground singlet state
S_1	first excited singlet state
S_2	second excited singlet state
T_1	first excited triplet state
TCO	transparent conductive oxide
TEM	transmission electron microscopy
TiO_2	titanium dioxide
TPP	tetraphenylporphyrin
TTA	triplet-triplet annihilation
V_{oc}	open-circuit photovoltage
ZnTPP	zinc (II) tetraphenylporphyrin
ZnTAPP	5, 10, 15, 20-tetrakis(4-aminophenyl)porphyrin-Zn(II)
ZnTCPP	5, 10, 15, 20-tetrakis(4-carboxyphenyl)porphyrin-Zn(II)
ZnTSPP	5, 10, 15, 20-tetrakis(4-sulfonatophenyl)porphyrin-Zn(II)

Chapter 1: Introduction

1.1 Overview

Dye-sensitized solar cells have gained considerable attention as one of many new technologies developed for alternative energy harvesting.[1] Although a number of different approaches have been attempted to improve solar-to-electrical conversion efficiencies for these photovoltaic devices, the use of photon upconversion holds significant potential for achieving this goal. Photon upconversion is a photophysical process that occurs when lower energy photons in the red or near-infrared (NIR) region of the optical spectrum are converted into higher energy photons. In this thesis, this has been achieved through the use of the triplet-triplet annihilation (TTA) mechanism. A key requirement for efficient TTA is aggregation of the sensitizer dye as two molecules are required for this process to occur. The purpose of this thesis was to evaluate the effects that the adsorption of porphyrin dyes onto a semiconductor would have on the spectroscopic properties of the porphyrin, and in particular, the ability of porphyrins to undergo photon upconversion via the triplet-triplet annihilation mechanism. The underlying theories essential to understanding photon upconversion are discussed in this chapter.

1.2 Introduction to photochemistry

The field of photochemistry deals with the variety of processes that result when light is absorbed by a molecule. The absorption of light is essential for numerous important reactions and processes to occur. When a molecule absorbs a photon of light it becomes promoted to a higher energy level, with the change in energy corresponding to the energy of the absorbed photon.

Each electronic state of a molecule is associated with a series of different vibrational states.[2] When absorption occurs, the molecule is typically promoted to a higher-energy vibrational state, but when in solution, rapidly returns to the ground vibrational state through vibrational relaxation. As illustrated in the simple state diagram shown in Figure 1.1, absorption results in a molecule reaching a higher vibrational level within each excited singlet state.

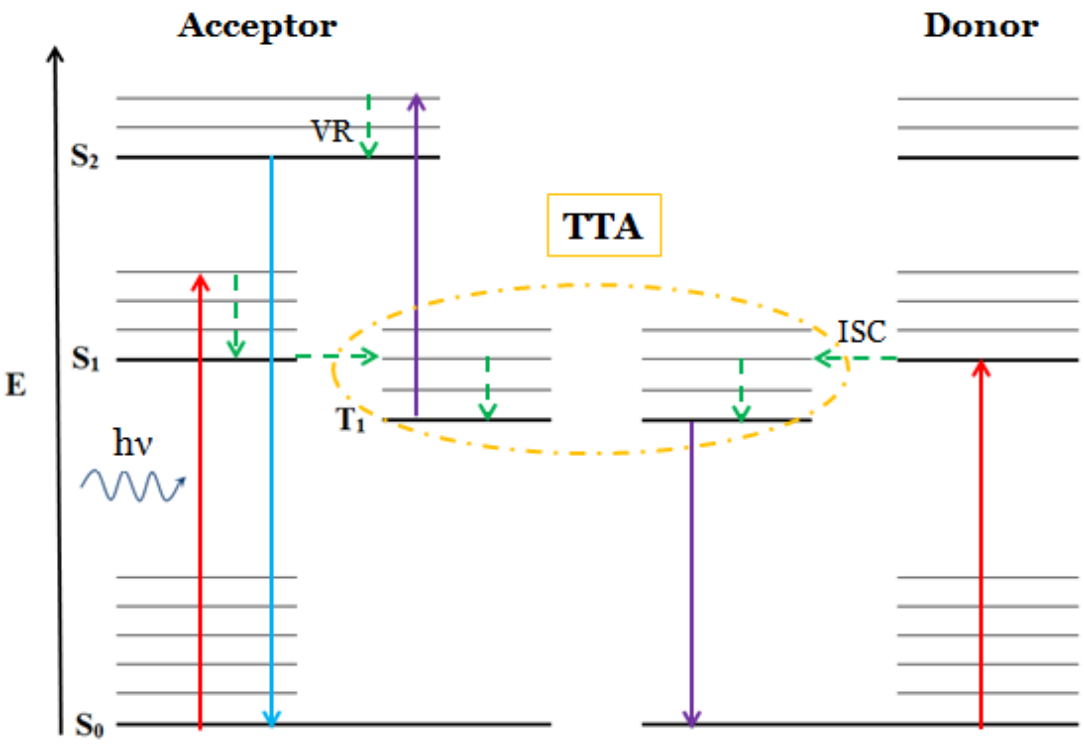

Figure 1.1 Jablonski diagram illustrating homomolecular triplet-triplet annihilation between an acceptor and donor molecule, where E denotes energy level, VR is vibrational relaxation, ISC is intersystem crossing, and TTA is triplet-triplet annihilation. Singlet states are labeled as S_0 (ground state), S_1 (first excited state), and S_2 (second excited state). The first excited triplet state is denoted as T_1.

When a molecule undergoes a radiative transition from an excited singlet state, S_n, where n = 1, to any vibrational level of the ground state (n = 0), the accompanying photon emission is called fluorescence. It is typically characterized by the rate constant, k_f, the quantum yield of fluorescence, Φ_f, and the energy of the released photon, $h\upsilon_f$. The fluorescence quantum yield is a very important property that is defined as the ratio of the amount of emitted fluorescence photons to photons absorbed.[2] The energy of the emitted photons is typically less than that of the absorbed photons. This relationship can be observed easily in the wavelengths of the emission, λ_{ems}, and absorbance, λ_{abs}, measured, where absorbance wavelength is generally shorter. The difference observed between the maximum wavelength of absorbance and emission is referred to as the Stokes shift, and is an important measure of the differences in electronic structure of the excited state and ground state.

Measuring the wavelength of absorbed and emitted light is one method used to assess electronic structures of molecules. The intensity of spectroscopic bands can also provide useful information on electronic structure, but fluorescence emission intensity can be easily affected by quenchers. Quenchers are molecules that reduce the intensity of emitted light, and quenching processes can occur as long as the quencher is in close proximity to the excited state molecule.[2] However, quenching processes can also provide useful information about the system, including, for example the ability of excited state molecules to exchange energy with their surroundings.[2]

In addition to radiative transition, photoexcited molecules can also undergo non-radiative transitions to lower energy levels in the form of either internal conversion (IC) or intersystem crossing (ISC). Internal conversion is a transition from a higher electronic state to a lower one

within the same spin state, for instance $S_2 \rightarrow S_1$. Intersystem crossing is a transition from a higher energy electronic state of one spin state to a lower energy state of a different spin state, for example $S_1 \rightarrow T_1$. One key transition is the formation of triplet states that follow the ISC pathway from an excited singlet state ($S_n \rightarrow T_n$). The excited triplet state possesses a higher spin multiplicity than its corresponding singlet state, which puts it at a lower energy level as stated by Hund's rule.

Although formation of triplet states occurs, ISC is classified as a quantum-mechanically forbidden transition, whereas IC of singlet states ($S_n \rightarrow S_0$) is an allowed transition. In fact, all processes involving transitions between singlet states and triplet states (T_n) are classified as forbidden pathways, such as $S_n \rightarrow T_n$ and $T_1 \rightarrow S_0$ (phosphorescence). A pathway is regarded as forbidden when the transitions are more improbable, or much slower to occur. It is thought that ISC is possible through spin-orbit coupling and is influenced by the electron's spin and orbital motions. This is significant because triplets are typically only formed through ISC. Additionally, triplet states tend to have longer lifetimes than singlet states because their transitions to ground singlet states are formally forbidden.[2]

1.3 Photon upconversion by triplet-triplet annihilation

Photon upconversion via triplet-triplet annihilation (TTA) has gained significant recent attention, since this process allows for light harvesting from the photon rich red and NIR region of the solar spectrum.[3] This is noteworthy due to its potential applications in dye-sensitized solar cells (DSSCs), where it can be used to collect photons that would otherwise not be absorbed and converted into electrical energy. Collecting additional photons is thought to have the potential to significantly increase conversion efficiency of photovoltaic devices. Systems that demonstrate

heteromolecular or homomolecular TTA have been studied in solution and solid-state, but have not yet been applied to photovoltaic devices.[3-8]

TTA is a photophysical process that can result in photon upconversion (shown in Figure 1.1). In this process, lower energy photons in the red or near-infrared (NIR) region of the electromagnetic spectrum are absorbed and then emitted as higher energy photons.[4] This occurs when two molecules occupying the lowest excited triplet state, T_1, interact resulting in one molecule (energy acceptor) being promoted to an excited singlet state, S_n (where $n \geq 2$), while the other (energy donor) returns to the ground singlet state, S_0. The upconverted fluorescence can be achieved through two different mechanisms that are dependent on the choice of donor and acceptor molecule. When the donor and acceptor is the same type of molecule (for example, two identical metalloporphyrins), the process is referred to as homomolecular, whereas when the donor and acceptor are different types of molecules (for example, a metalloporphyrin and a small organic acceptor), the process is referred to as heteromolecular TTA. In either case, the donor and acceptor must have long triplet lifetimes and a large S_1-T_1 energy gap in order for upconversion to be efficient.[4] This is important because upon excitation to the S_1 state, the donor will undergo ISC to its excited triplet state, T_1. The energy of the excited donor molecule is transferred to the acceptor via a non-radiative process, which is dependent on distance separating the molecules involved, restoring the donor to its ground state. If the acceptor also exists in its excited triplet state it annihilates to the S_2 state, a process that relies on the S_2-S_0 and T_1-S_0 energy gaps of the donor and acceptor.[3,9] The resulting $S_2 \rightarrow S_0 + h\nu$ upconverted fluorescence via TTA is delayed.

In this thesis, porphyrins were chosen as a sensitizer due to their ability to undergo upconversion by a homomolecular TTA mechanism.[4,5] In particular, the use of closed-shell

metalloporphyrins allows for excitation in the visible absorption region to produce the lowest excited singlet states, S_1, which in turn is capable of efficient ISC (triplet quantum yield approaching 1) into the T_1 state.[4] The long-lived triplet states ensures that the triplet population is high enough for TTA to occur efficiently and that a measurable S_2 fluorescence is produced.[3,4] In addition, energy transfer between the donor and acceptor is affected by distance and by orientation of the molecules.[10] Porphyrins are known to readily form H-aggregates (face-to-face) or J-aggregates ('slipped' face-to-face), which are two orientations that allow for efficient energy and electron transfer (Figure 1.2).[10-13]

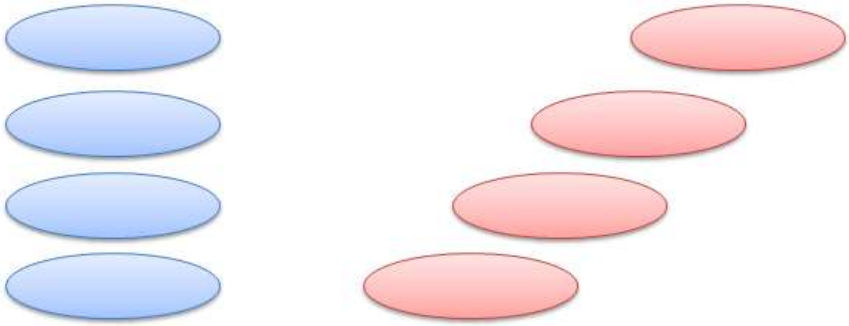

Figure 1.2 Illustration of H-aggregate (shown left) and J-aggregate (shown right).

1.4 Porphyrins

Porphyrins are a large family of macrocyclic aromatic molecules, the basic chemical structure of which is shown in Figure 1.3. Although porphyrins are typically planar, the binding of metal atoms in the centre position or further protonation of the central nitrogen atoms can lead to structural distortions.[14] Distortions of the macrocycle also occur with addition of substituents

onto the carbons or nitrogens. The introduction of such variations to the porphyrin ring results in these molecules having a wide range of photophysical properties and biochemical functions.

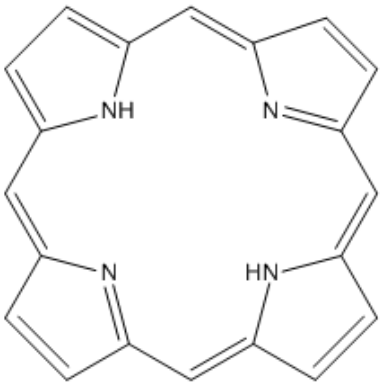

Figure 1.3 Typical chemical structure for an unsubstituted, non-metallated macrocyclic porphyrin.

The effects of varying the electronic structure of porphyrins can be seen in the diverse biochemical roles observed for porphyrins of different structures. For instance, heme, vitamin B12 and chlorophyll have similar porphyrin-like ring structures, but have entirely different biochemical and photophysical properties. The coordinating metal is responsible for the electronegativity of the porphyrin, and substituents on the ring affect aromaticity and photochemical properties.[14]

Chlorophyll is just one example of a porphyrin-related molecule, but an important one that utilizes bulky substituents to harvest solar energy for photosynthesis. Arranged into an antenna formation, the conjugated substituents transport excitons (mobile excited states) to the metal centre of the ring. Although naturally occurring porphyrins serve important roles in

sustaining life, synthetic porphyrins have also been developed for applications in electronics, medicine, and alternative energy.[14]

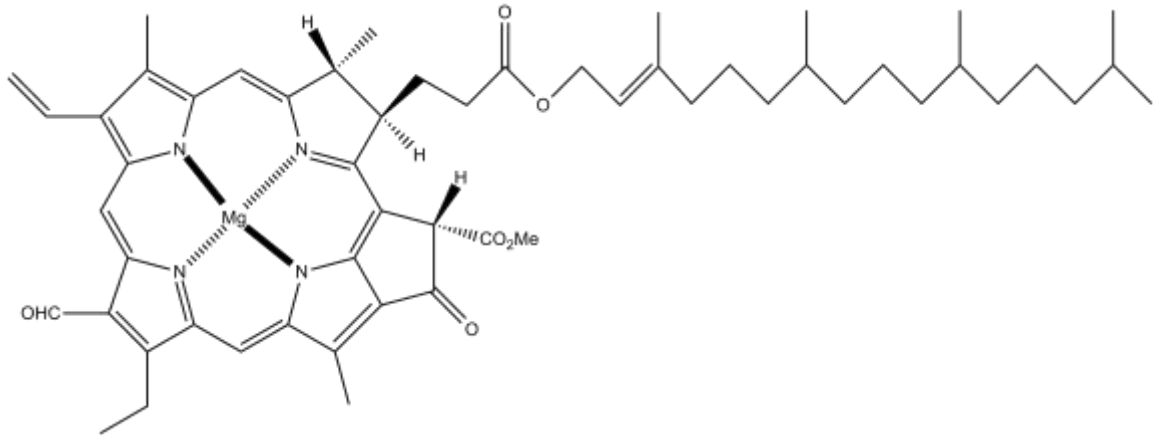

Figure 1.4 Chlorophyll B structure (adapted from reference 13).

Porphyrins can be used for light-harvesting applications, and are well-known for forming antenna-like structures. The tunability of the porphyrin ring makes it ideal to achieve desired optical properties. By extending the π-system, porphyrins can be engineered to behave similarly to natural systems that carry out photosynthesis. Among the porphyrins, tetraphenylporphyrin (TPP) and octaethylporphyrin (OEP) are the most widely studied and used. Additionally, these porphyrins are relatively inexpensive, and TPP is the simplest porphyrin to synthesize.

Several models have been developed that attempt to predict porphyrin absorption spectra. The absorption ability of porphyrins varies depending on substitution of the centre position, e.g. free-base (vacant central position), monocation, dication, or metal complex, and the position of ligands on the macrocycle (e.g. *meso*- or β-substituents). The typical porphyrin absorption spectrum is characterized by two intense absorption bands in the 390-425 nm range, referred to

as B bands or Soret bands, and two or four weaker bands observed in the region 480-700 nm, referred to as Q bands (Figure 1.5).[14] The absorption bands observed are a result of vibrational and rotational changes when the molecule undergoes single-electron excitation during a $\pi \rightarrow \pi^*$ transition. Within a series of porphyrin analogues, the position of absorption bands are influenced by the type and location of the ligands found on the ring. The relative intensities of these bands are indicators of ligand positions around the macrocycle and presence of a metal centre.[14]

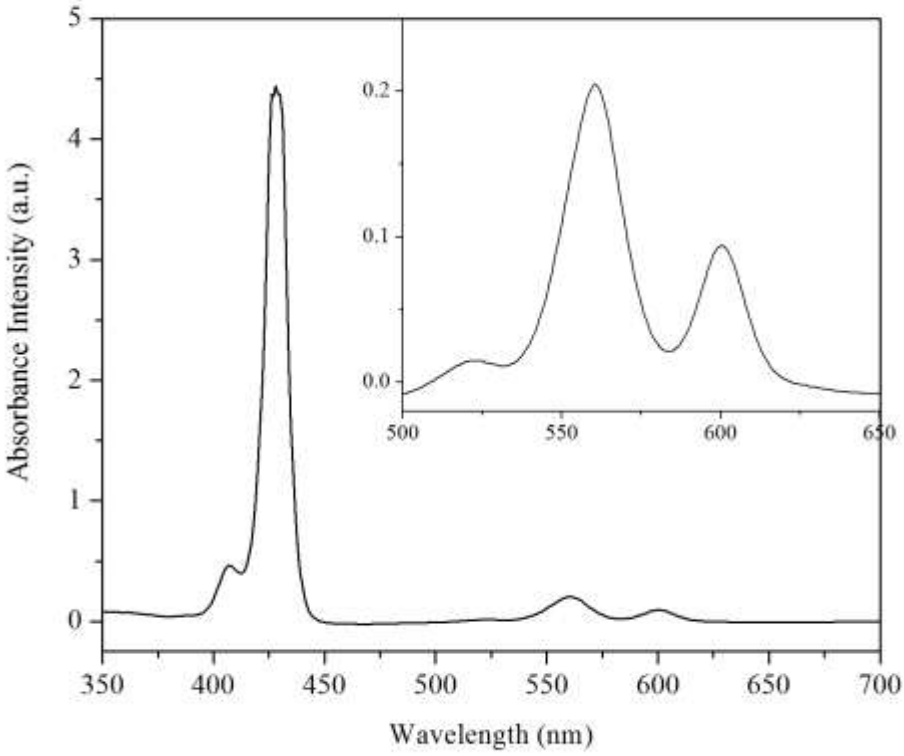

Figure 1.5 Typical absorption spectra of porphyrin (shown is 10 µM ZnTCPP in ethanol). The band at ~ 425 is the Soret band and the bands at ~560 nm and 600 nm are the Q-bands. The Q-bands are shown in higher resolution in the inset.

In metal complexes, only two Q bands are observed, rather than the four found in the absorption spectra of free-base porphyrins, and are labeled separately as α- and β-bands. The β-band is found at a shorter wavelength relative to the α-band. The relative intensity ratio of these two bands can be used as an indicator for the stability of the metal-nitrogen complex, which is largely influenced by the choice of metal. For instance, a small α to β band intensity ratio is indicative of low stability of the metal complex in some metalloporphyrins. The use of a transition metal also introduces additional bands due to other types of electron transfers, such as metal-to-ligand charge transfer (MLCT) or ligand-to-metal charge transfer (LMCT).[1,15] This can be eliminated by using a closed-shell metal.

The number of valence electrons in the metal centre determines whether the absorption and emission spectra of the metalloporphyrins can be classified as "regular" or "irregular".[14] The normal spectra of "regular" metalloporphyrins are characterized with the B bands occurring at 390-425 nm, and α and β positions of the Q band found at 570-610 nm and 590-630 nm, respectively. However, "irregular" metalloporphyrins typically give three different types of spectra: normal, hypso, and hyper.

Hypso-type spectra are characterized by hypsochromically shifted (blue-shifted) B and Q bands. This is typically achieved by a metal-to-ring charge transfer from elements of group 8 to 11, which increases the energy observed from the single-electron $\pi \rightarrow \pi^*$ transition within the porphyrin macrocycle. This increase in energy is responsible for the blue-shift observed in the bands. Metal substituents that give rise to this are Ni (II), Pt (II) and Pd (II). Hyper-type spectra are found to contain additional absorption bands, which are used to further classify this type of spectra into two different categories depending on the type of electron transition.

The most robust model used to predict absorption and emission spectra for porphyrins is the four-orbital model, which was developed by Gouterman in 1961.[14] The four-orbital model only considers contributions from the two highest occupied molecular orbitals (HOMOs) and lowest unoccupied molecular orbitals (LUMOs). While a simplified model, it successfully predicts the number of bands, their multiplicities, and their relative intensities. Additionally, it also takes into account the effects of having a metal centre on the overall symmetry of the porphyrin macrocycle. Several other theories were developed prior to this particular model but were incomplete in their predictions. The four-orbital model unifies aspects from the other models into a more encompassing approach to interpreting porphyrin spectra.

1.5 Dye-sensitized solar cells

Photovoltaics can be broadly classified as belonging to one of three different categories (1^{st}, 2^{nd} or 3^{rd} generation) depending on the technology that was used to develop the devices. Single junction photovoltaics were an inspiration for the development of first and second generation devices. Third generation photovoltaics is a term generally used to refer to recent developments in technologies used; however, current dye-sensitized solar cells (DSSCs) are viewed as being a stepping stone toward the development of third generation devices, which are expected to be offered at a competitive price compared to other photovoltaics on the market. Although, the research and development within the area of photovoltaic technologies has grown rapidly in recent years, the costs to develop DSSC devices do not compare with silicon-based solar cells.[1,16]

The DSSC is regarded as one of the most promising areas of technological development in alternative and renewable energy sources.[1,16-25] Considering that the mean global energy

consumption was estimated to be 13 TW in 2000, and is projected to increase to 28 TW by 2050, it is essential to find a source of renewable energy to meet future needs. Solar energy is the most promising and largest source of potential energy, with about $1.7 \cdot 10^5$ TW reaching the earth's surface each year and 600 TW being viable terrestrial energy.[26] The DSSC has been found capable of efficiently converting solar energy, with growing investments and efforts to increase this efficiency and reduce production costs.[1,19,20,26-29]

A standard DSSC set up is shown in Figure 1.6. This type of cell is driven by electron transfer, which begins with excitation of the sensitizer. The excited electrons from the sensitizer are then transferred into the conduction band of the semiconductor, where they will be transported to the transparent conductive oxide (TCO), which facilitates current towards external circuit. The oxidized sensitizer dye is reduced by the electrolyte, which serves the role of redox mediator.[30] However, the rate at which dye regeneration occurs affects the overall efficiency of the cell. If this particular process is slower than charge injection into the semiconductor, then the excited dye electron has an opportunity to recombine with another oxidized sensitizer. Additionally, excited sensitizer electrons are also able to react with the electrolyte if the distance between the charge injection site of the semiconductor and the TCO is too long.[26] This reduces the total electrons available to be transported into the external circuit. Electrons will travel towards the counter electrode, where they are used to replenish the electrolyte, which is required for dye regeneration to occur. Working efficiency of this type of cell is based on the choice of sensitizer, semiconductor, transparent conductive oxide (TCO), electrolyte and construction method.[26,31]

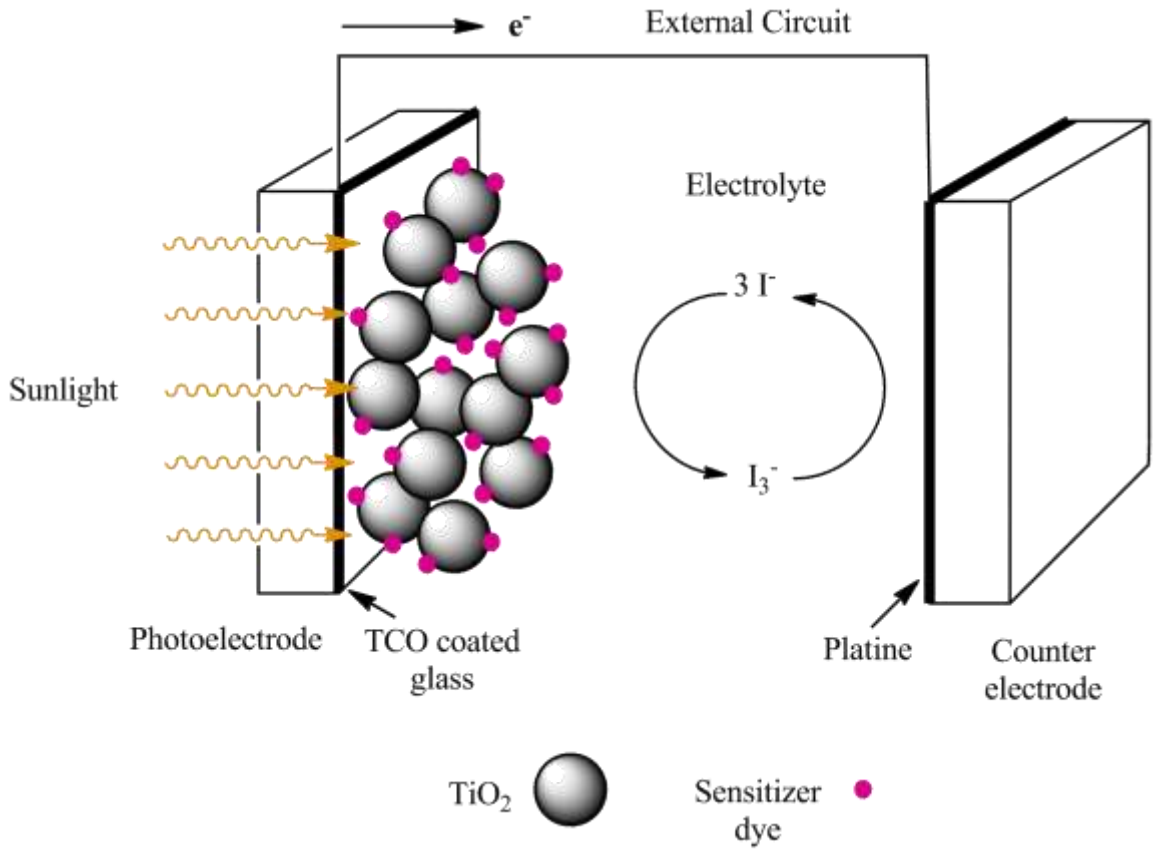

Figure 1.6 Schematic of a dye sensitized solar cell (adapted from reference 32).

Despite the apparent simplicity of the electron transfer processes described above, the intricacies of the various components that compose the cell must be understood for optimum cell performance. The most important components are the sensitizer dye, since it is essential for the electron injection to take place, and the semiconductor, which is required to transfer the electrons into the external circuit. For this reason, dye adsorption is an important factor in dictating DSSC conversion efficiencies and large semiconductor surface areas are necessary for improved sensitizer loading. The need to fulfill this requirement has led to researching different methods for synthesizing mesoporous, high surface area semiconductor sol-gel materials.

A common method for synthesizing mesoporous semiconductor frameworks is the use of block copolymers to template sol-gel materials.[32-34] It has been found that organized mesoporous TiO_2 thin-films have about 50% more solar-conversion efficiency than TiO_2 films made from randomly oriented nanoparticles.[32] In addition, the rough surfaces associated with these films have been found to improve device performance under diffuse light conditions.[35] Furthermore, fabrication of DSSCs does not require high purity of materials and can be carried out in a normal lab setting, unlike semiconductor photovoltaics which require a highly pure composition with minimal defects and interfaces that interfere with the separation of electron-hole pairs.

Numerous DSSC systems have been studied thus far, in an attempt to find the combination of dye, electrolyte and semiconductor that provides the best conversion efficiencies. As a result, various types of dyes, electrolyte systems, and different compositions and morphologies of mesoporous semiconductor thin films have been investigated in literature.[21,24,26] The influence that each DSSC component has on the overall performance of the system provides opportunity to focus efforts on improving just one component or a combination. This research will focus on investigating the sensitizer and the capability of sensitizer to give rise to TTA.

The ultimate goal of DSSC research is to maximize photon conversion efficiencies. Referring back to the electron transfer processes briefly outlined, efficiency is an indication of how well the cell can transfer the captured photon energy through the many junctions (sensitizer/electrolyte/semiconductor/TCO) into the external circuit. Conversion efficiencies are important indications for DSSC performance, and are commonly reported using two different measurements. The solar-to-electrical energy conversion efficiency, η, is one measure of performance. It is determined using the short-circuit photocurrent density (J_{sc}), open-circuit photovoltage (V_{oc}), the fill factor (FF) and intensity of the incident light (P_{in}):[26]

$$\eta = \frac{J_{SC} V_{OC} FF}{P_{in}} \qquad \text{(Eq 1.1)}$$

J_{sc} is determined when voltage is 0 V, and V_{oc} is found when current is 0. The fill factor is a ratio of the maximum power of the solar cell (P_{max}) and the product of J_{sc} and V_{oc}. It can be any value between 0 and 1, and describes the current-voltage (*I-V)* curve.[26] The closer this value is to 1, the more rectangular the current-voltage curve will appear. As the number of electrons lost through the various electron transfer processes increases, the FF value will decrease, and the *I-V* curve will become more rounded in appearance.[26] The other measure of performance is the incident photon-to-current conversion efficiency (IPCE), which is the J_{sc} in the external circuit divided by the cell's exposure to the photon flux. This particular measurement is an important value indicating the monochromatic quantum efficiency – the spectral response of the system.

Investigations aimed at improving cell performance are typically focused on developing dyes and dye systems that are successful in harvesting solar energy as a monomolecular layer or thin-film. Efforts to fabricate cells with multiple layers of dye with improved efficiencies were overall unsuccessful.[26] The most efficient DSSCs are reported to have reached 11% efficiency using ruthenium polypyridyl complexes.[25] Although Ru(II) complexes are found to be most efficient sensitizers, other organic dyes are being studied or engineered, including porphyrin systems.

Porphyrins are thought to be a promising sensitizer, largely due to the role of porphyrin derivatives in photosynthesis, and relatively low cost compared to other commonly used sensitizers, such as Ru-containing dyes. Additionally, some porphyrins are found to possess high extinction coefficients in the near-IR region. The need to develop sensitizers that absorb

strongly in the IR and near-IR is necessary in order to achieve efficiencies above 15%.[26] The best efficiency achieved with a porphyrin-sensitized solar cell is reported to be 7.1%.[25]

1.6 Research objectives

The goal of this research was to investigate potential application of TTA as a method to improve DSSC efficiencies. Additional efforts were made to synthesize mesoporous TiO_2,[32-34] as it provides the large surface area needed for dye loading,[20,32] allowing for sensitization with a dye capable of exhibiting TTA. To provide rapid charge injection, it has been found that a dye must be strongly bound to TiO_2 through functional groups, such as carboxylic acids, and that varying these linker groups can be used to optimize cell performance.[36] In order to facilitate efficient transfer of electrons into the conduction band, functionalized versions of the metalloporphyrin, Zinc tetraphenylporphyrin (ZnTPP) were used (Figure 1.7). This relatively cheap dye has been found to absorb in the red and NIR region, and exhibit S_1-S_0 (Q band) and S_2-S_0 (Soret/B band) fluorescence; as such, spectroscopy of ZnTPP has been studied thoroughly.[37] However, the intensity of the delayed S_2 fluorescence in solution has been found to be dependent on the formation of aggregates.[4]

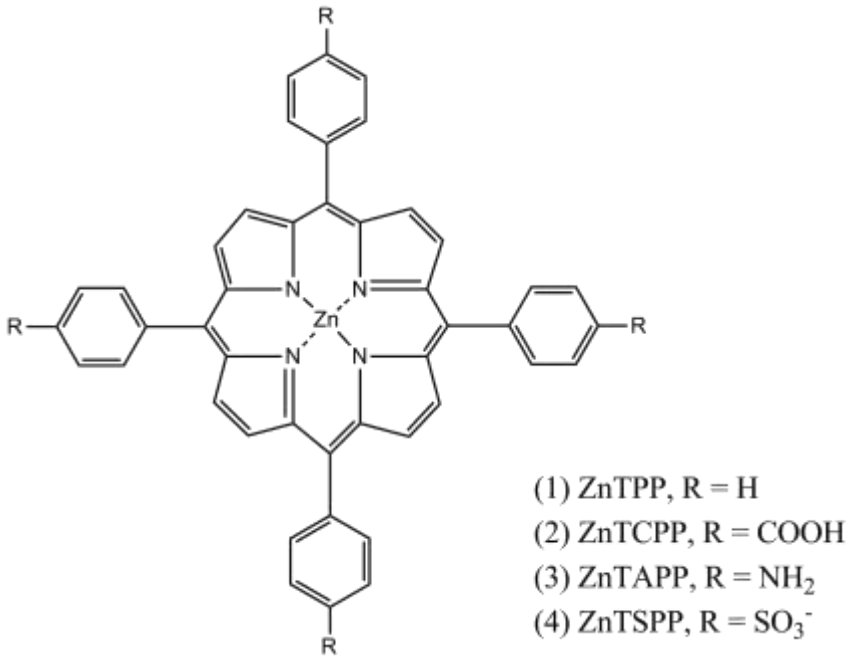

Figure 1.7 Chemical structures of the zinc (II) porphyrins used in this study.

In DSSCs, however, it has been found that the formation of aggregates leads to increased charge recombination, which results in fewer electrons being carried through the external circuit. This is contrary to studies of porphyrins capable of undergoing TTA that have determined that aggregation is critical for upconversion to occur. Controlling aggregation then becomes crucial for upconversion by TTA to be a feasible option for improving efficiencies in DSSCs. It is predicted that using ZnTPP with linker groups should hinder aggregate formation due to increased steric bulk. In addition, the presence of functional groups allows the porphyrins to bind to the Ti^{4+} centre more efficiently than porphyrins that lack these groups. This should allow more electrons to be transferred efficiently to the semiconductor.

The dyes 5, 10, 15, 20-tetrakis(4-aminophenyl)porphyrin-Zn(II) (ZnTAPP); 5, 10, 15; 20-tetrakis(4-sulfanatophenyl)porphyrin-Zn(II) (ZnTSPP); and 5, 10, 15, 20-tetrakis(4-

carboxyphenyl)porphyrin-Zn(II) (ZnTCPP) were used in this research (as shown in Figure 1.7). The porphyrins were initially studied in solution phase by measuring absorbance and emission spectra, and compared to those of ZnTPP. This was primarily done to verify S_2 emission capabilities (Chapter 2). This was followed by measurements conducted using sensitized TiO_2 thin-films and evaluating porphyrin solid-state optical properties. Efforts were made to measure upconverted fluorescence of the thin-film samples as these results may have an influence on future research involving the potential use and application of TTA in photovoltaics (Chapter 3). Crude DSSCs were then assembled to gather preliminary data on the performance of the porphyrins as sensitizers (Chapter 4). The results from these experiments are presented and discussed in this thesis.

Chapter 2: Spectroscopic Properties of Metalloporphyrins in Solution

2.1 Overview

Solution-based spectroscopic measurements have been carried out in order to determine the effectiveness of functionalized Zn (II) porphyrins as sensitizers compared to the model reference compound ZnTPP. The focus of this study was to determine whether the functionalized Zn (II) porphyrins were capable of undergoing triplet-triplet annihilation. The results gathered from the steady-state absorption and emission measurements are presented and discussed in this chapter.

2.2 Materials and Methods

Chemicals

All chemicals and solvents were used without further purification. ZnTPP was obtained from Sigma-Aldrich. ZnTAPP and ZnTCPP were purchased from Porphyrin Systems. ZnTSPP was obtained from Frontier Scientific, Inc. All solvents used (ACS grade) were purchased from EM Science (toluene), VWR (methanol), and Commercial Alcohols (100% ethanol [EtOH]). Millipore filtered water (MilliQ Gradient; resistivity 18.6 MΩ·cm) was used from a Milli-Q purification system.

Sample Preparation

Porphyrin solutions of 1 and 10 μM concentration were prepared for steady-state absorption measurements. The steady-state fluorescence and upconverted fluorescence measurements were carried out at room temperature using 10 μM and 200 μM solutions, respectively. Because of different solubilities, each porphyrin solution was prepared using a

different solvent. ZnTPP, ZnTAPP, ZnTSPP and ZnTCPP were dissolved in toluene, acetone, water, and methanol, respectively. The 10 μM solution of ZnTCPP used for collection of the steady-state emission spectrum was prepared in DMSO. Solutions for upconverted fluorescence measurements were degassed using Schlenk line techniques and a vacuum pump prior to collection of spectra.

Instrumentation

Absorption spectra were recorded with a Varian Cary 500 Scan UV-Vis-NIR spectrophotometer using 10 mm x 10 mm quartz cuvettes. Fluorescence spectra were recorded with a Photon Technology International spectrofluorometer, and upconverted fluorescence measurements were carried out in the same spectrofluorometer but using a CW 532 nm Nd:YAG laser for excitation. All fluorescence measurements were carried out in a 2 mm x 10 mm cuvette. For upconverted fluorescence measurements, following excitation by 532 nm, spectra were collected in the ranges of 400 – 500 nm (for the B-band) and 550 – 750 nm (for the Q-band). The illuminating power of the laser was controlled using an optical density filter before excitation of sample, and a notch filter was used to remove scattered laser light. For fluorescence measurements, the solutions were excited at 400 nm and collected in the 410 – 750 nm range. Absorption spectra were collected in the 350 – 700 nm range. All measurements were carried out at room temperature.

2.3 Results and Discussion

2.3.1 Absorption spectra measurements

The well-known spectroscopic properties of ZnTPP made it a suitable choice for a reference to gauge the behaviour of the functionalized Zn (II) porphyrins in solution. The two different concentrations of Zn (II) porphyrins were prepared as described in the Sample Preparation section above. The resulting spectra for 10 µM and 1 µM solutions are presented in Figure 2.1 and 2.2, respectively.

The absorption spectra shown in Figure 2.1 and 2.2 were characterized by two low intensity bands between 530 – 630 nm corresponding to the Q bands. The first Q band is referred to as Q(0-0), and is found at a lower wavelength corresponding to a transition from the ground vibrational energy level of S_0 to the ground vibrational energy level of S_1. The second Q band is an excitation from the S_0 ground vibrational energy to first vibrational energy level of S_1, and is denoted as Q(0-1). Large intensity bands were also observed between 385 – 460 nm corresponding to the porphyrins' Soret band. The Soret bands exhibited a small shoulder in the shorter wavelength region. Figure 2.1 was normalized to allow for easier comparison of the porphyrin absorption spectra and their characteristic bands. In this spectrum, the ratios of band intensities were similar between all porphyrins when comparing the Soret band with the Q bands. Figure 2.2, however, was not normalized and was found to depict the effects of the solvent and solute interactions.

The similar features that exist between ZnTPP and its functionalized derivatives are seen in Figure 2.1. However, the Soret and Q bands of the functionalized porphyrins were found to be spectrally shifted compared to the ZnTPP spectra. ZnTSPP exhibited a red shift, and a blue shift

was observed with ZnTAPP and ZnTCPP. This might be attributed to the fact that each porphyrin solution was prepared using different solvents. The differences in solubility made it difficult to reduce solvatochromic effects that are bound to arise when using different solvents. Typically, aggregate formation results in spectral shifts,[38] but in this case, it is difficult to dismiss solvatochromic effects. Additionally, the functional groups will affect the π system of the porphyrin macrocycle, depending on its electron donating or withdrawing nature.[39] As mentioned briefly in the previous chapter, the optical properties of porphyrins are tunable by substituting different functional groups around the ring at different positions.[14] The spectral shifts that were observed may largely be due to this property since changing the ligand changes the molecule, which will result in different spectra. Absorbance spectra were collected using solutions varying from 0.5 μM and 2.5 μM, and for two of the functionalized porphyrins, upwards to 5 μM. No spectral shifts were observed in these measurements or when comparing Soret and Q bands between Figure 2.1 and 2.2. This is an indication that the spectral shifts observed between porphyrins were not due to increased aggregate concentration.

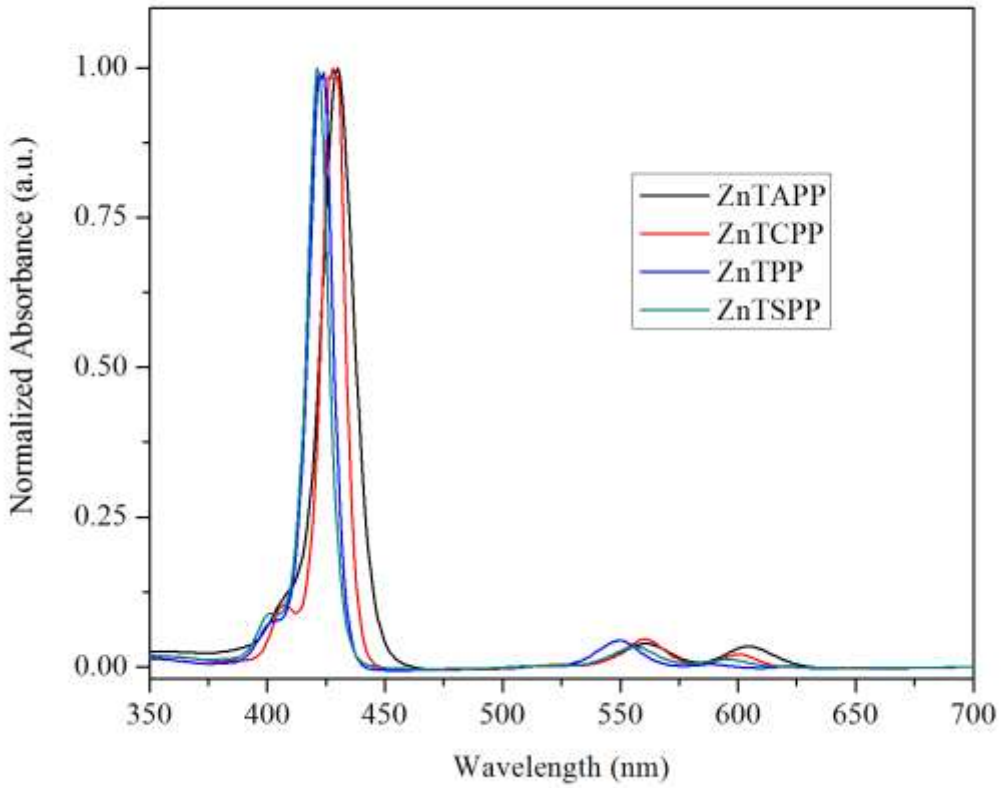

Figure 2.1 Normalized absorption spectra of 10 μM Zn (II) porphyrin solutions in different solvents. ZnTAPP, ZnTCPP, ZnTPP and ZnTSPP solutions were prepared in acetone, methanol, toluene and water, respectively.

After normalizing the spectra, it was evident that there were variations in peak widths (described by the full-width at half maxima (FWHM)). Band broadening suggests formation of aggregates and an increase in aggregate concentration.[40-42] ZnTAPP displayed the largest peak width (~16 nm) in comparison to ZnTPP (~12 nm). The FWHM of ZnTCPP (~11 nm) and ZnTSPP (~10 nm) were more comparable with that of ZnTPP. This suggested that ZnTAPP

aggregated more than ZnTPP or the other functionalized porphyrins, ZnTCPP and ZnTSPP. The higher aggregate concentration of the amino substituted porphyrin may have been due to relatively stronger solute-solute interactions. Similarly, the anionic nature of the functional groups found in ZnTCPP and ZnTSPP may have attributed to stronger repulsion between porphyrins, thus hindering aggregate formation. As mentioned previously in the Introduction (Chapter 1), aggregate formation is required for upconversion by triplet-triplet annihilation (TTA) to occur readily. This is particularly important as it has potential to enhance the performance of sensitizers in dye-sensitized solar cells (DSSCs).

The variations in relative band intensity and spectral shifts observed provide further information regarding aggregation behaviour. When comparing the Q bands between spectra, an increase in the Q band intensity was observed for ZnTCPP, which may have been due to the presence of aggregates.[40] The significant red shifts of the Q band peaks for ZnTAPP (~11 and 17 nm, λ_{max} = 561 and 605 nm) from ZnTPP, apparent in Figure 2.2, suggested that this porphyrin aggregated more readily than ZnTCPP (~7 and 9 nm, λ_{max} = 557 and 597 nm) and ZnTSPP (~6 and 6 nm, λ_{max} = 556 and 594 nm). This supported the results obtained from comparing FWHM, which suggested that ZnTAPP was capable of aggregating more than the other porphyrins. This could also be due to interactions between the solutes and their respective solvents.

In literature, carboxyl-functionalized porphyrins display greater aggregating capabilities and are usually the preferred sensitizers for DSSCs.[19,41,43] However, the results from the steady-state absorption study indicated that ZnTAPP aggregated more than ZnTCPP. Spectral shifting and the FWHM data indicated that ZnTAPP aggregates more. ZnTCPP was found to have a slightly larger spectral shift from ZnTPP compared to that of ZnTSPP, which as mentioned

previously, could be used as an indicator for aggregate formation. As a porphyrin that was found more capable of aggregating, ZnTCPP also possesses functional groups that extend the conjugated π system of the macrocycle, which aides improved charge injection into the semiconductor.[39]

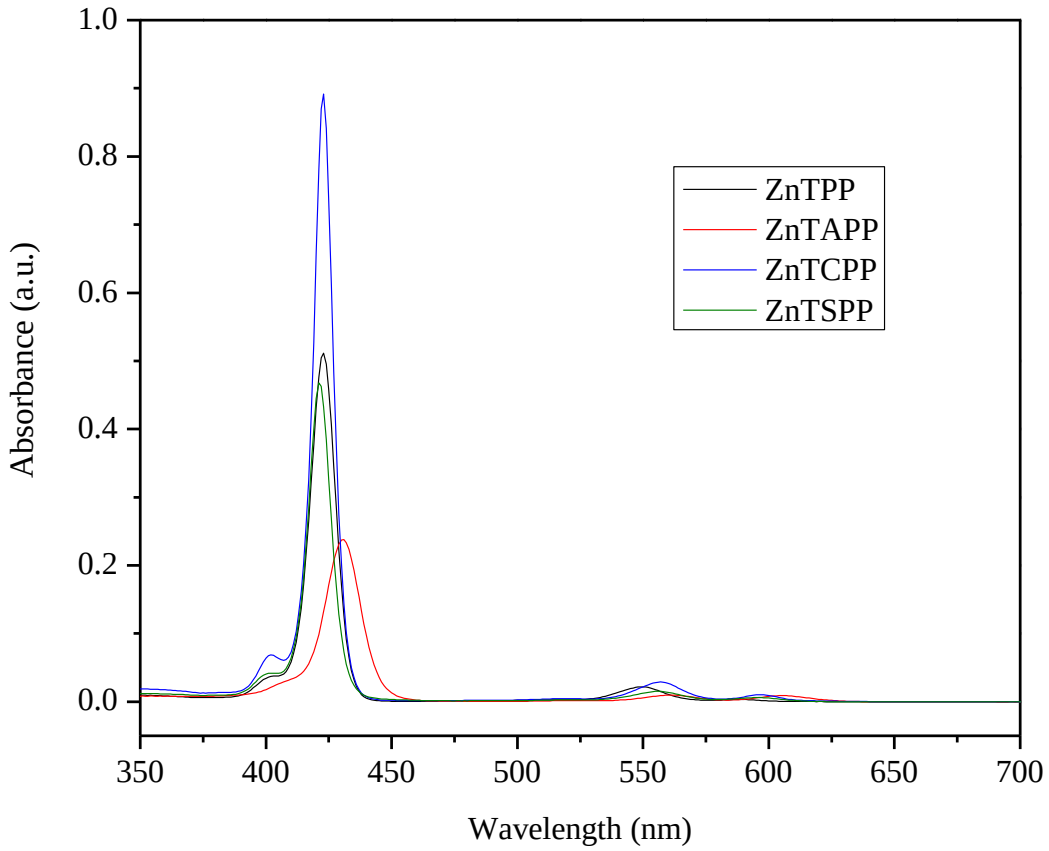

Figure 2.2 Corrected absorption spectra of 1 μM Zn (II) porphyrin solutions in different solvents. ZnTPP, ZnTAPP, ZnTCPP, and ZnTSPP solutions were prepared in toluene, acetone, methanol, and water, respectively.

A comparison of the experimental steady-state absorbance peak positions with those found in literature is provided in Table 2.1. In order to eliminate solvent effects, the literature values listed in the table were obtained from sources that used the same solvents for solution preparation that were used in this study. The only exceptions are the literature values listed for ZnTAPP, which were collected with solutions prepared with DMF rather than acetone. However, literature typically reported data for ZnTAPP solutions prepared in protic polar solvents, rather than an aprotic polar solvent, such as that used in the collection of experimental data. The experimental absorbance data collected in our measurements are clearly in good agreement with the literature values. Slight differences in absorbance maximum values may be attributed to instrumental response and effects that concentration have on aggregate formation.[4]

Table 2.1 Comparison of solution UV-Vis absorbance data of porphyrins with literature values.

Porphyrin	Soret λ_{max} (nm)		Q(0-0) λ_{max} (nm)		Q(0-1) λ_{max} (nm)	
	Exp	Lit	Exp	Lit	Exp	Lit
ZnTPP[a]	423	423	550	549	588	588
ZnTAPP[b]	431	437	561	567	605	614
ZnTCPP[c]	423	424	557	557	597	597
ZnTSPP[c]	421	421	556	555	594	594

Literature values taken from [a] Danger *et al.*[44], [b] Araghi *et al.*[45], [c] Rochford *et al.*[41], and [d] Neta *et al.*[46]

2.3.2 Emission spectra measurements

The steady-state emission spectra for the porphyrin solutions exhibited two bands. One band was observed between 300 – 460 nm corresponding to the Soret band emission, and the other was observed between 550 – 700 nm, corresponding to Q band emission. The Q bands consisted of two peaks centred at ~610 and 660 nm and the Soret peak was centred at ~440 nm,

with each porphyrin exhibiting different emission intensities. With the exception of ZnTPP, the Q(0-1) band peak (Q band located at the shorter wavelength) had a larger relative intensity than the Q(0-0) peak (longer wavelength Q band). The larger Q(0-1) band is expected because the 0–0 dipole transition is "forbidden" as stated by Franck-Condon principle.

The relative emission intensities of the Q bands were found to be larger than that of the Soret bands. The functionalized porphyrins were also found to have lower emission intensities for both the Soret and Q bands compared to that of ZnTPP. The ratios of the peak intensities for the Q(0-1) peak to the Soret varied significantly, with ZnTPP having the smallest ratio (~3:1) and ZnTSPP having the largest ratio (~59:1). ZnTAPP (~9:1) and ZnTCPP (~12:1) were comparable to ZnTPP, but still differed significantly. These relationships indicated differences in population of excited states between the different porphyrins.

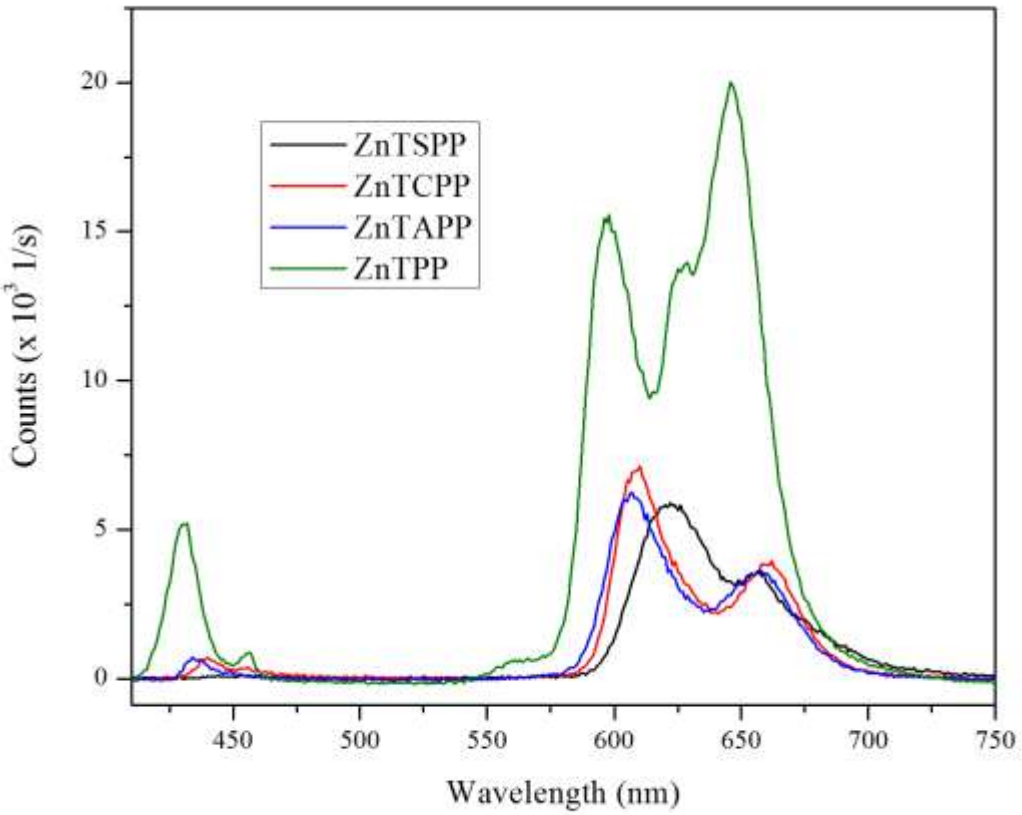

Figure 2.3 Steady-state fluorescence emission spectra of 10 μM Zn (II) porphyrins in different solvents. ZnTPP, ZnTAPP, ZnTCPP, and ZnTSPP solutions were prepared in toluene, acetone, DMSO, and water, respectively.

Table 2.2 compares the experimental emission peaks with those reported in literature. Once again the Q band emission maxima are very similar. However, the Soret emission of ZnTPP and ZnTSPP are significantly red shifted from literature values. Danger *et al.* and Szmytkowski *et al.* used concentrations of 5 and 1 μM, respectively. The larger concentration (ie. 10 μM) used in this study may have resulted in an increase in aggregate concentration, which

is typically observed through spectral shifting and band broadening.[13] The presence of an additional peak at ~630 nm for ZnTPP could be a verification of increased aggregation. The presence of more ZnTPP aggregates could have made it possible for population of other vibrational states to occur, resulting in the presence of the additional peak.

Table 2.2 Comparison of solution emission data of porphyrins with literature values.

Porphyrin	Soret λ_{max} (nm)		Q(0-0) λ_{max} (nm)		Q(0-1) λ_{max} (nm)	
	Exp	Lit	Exp	Lit	Exp	Lit
ZnTPP[a]	441	431	649	649	600	597
ZnTAPP	456	-	678	-	623	-
ZnTCPP[b]	440	-	658	658	606	606
ZnTSPP[c]	440	428[d]	657	656	607	606

Literature values taken from [a] Danger *et al.*[44], [b] Rochford *et al.*[41], [c] Kalyanasundaram *et al.*[47], [d] Szmytkowski *et al.*[48]

The upconverted S_2 emission spectrum (Figure 2.4) of the porphyrins was characterized by a band found between 420 – 480 nm, with a single peak near 440 nm. Unlike the Soret bands collected from the steady-state fluorescence measurements, the upconverted S_2 emission peaks exhibited strong band broadening and asymmetry. The functionalized porphyrins were also found to exhibit significantly weaker emission intensities than that of ZnTPP.

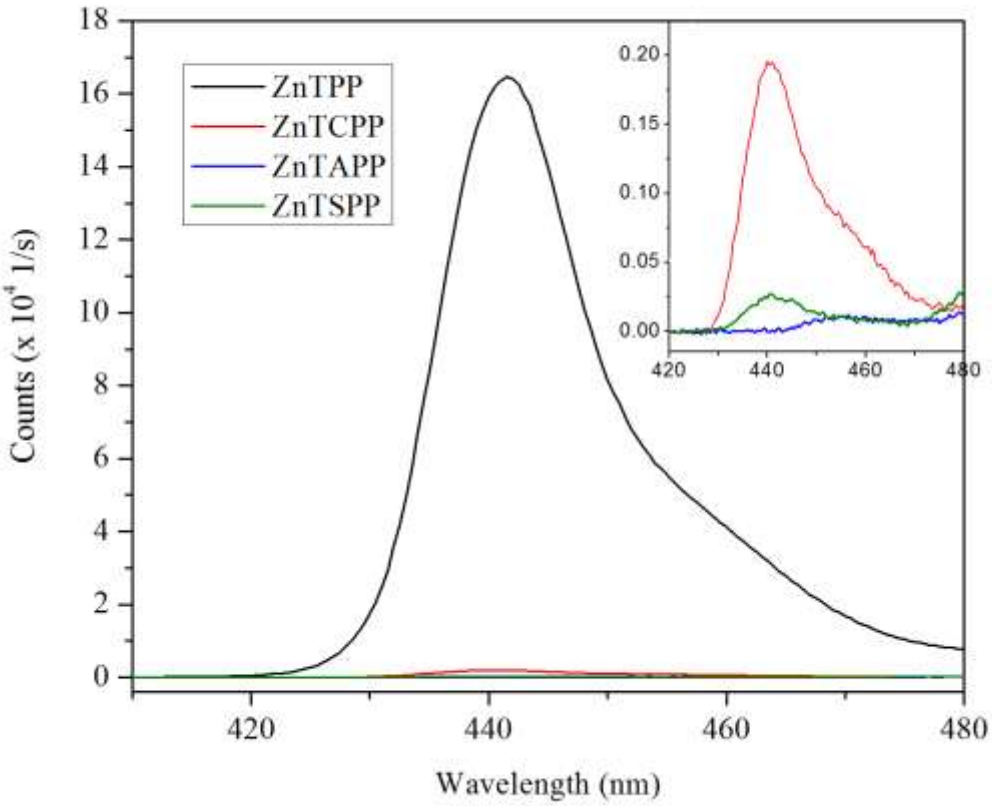

Figure 2.4 Upconverted S_2 emission spectra of 200 μM Zn (II) porphyrins in different solvents (λ_{ex} = 532 nm). ZnTPP, ZnTAPP, ZnTSPP and ZnTCPP were dissolved in toluene, acetone, water, and methanol, respectively. Inset shows an expanded scale spectrum for the functionalized porphyrins from 420 – 470 nm.

Unlike the Soret bands, emission intensities of the Q bands for the degassed samples (Figure 2.5) were comparable with those measured in the fluorescence emission experiments (Figure 2.3). The bands are found between about 575 and 725 nm. The peaks for the Q(0-1) and Q(0-0) bands were found to occur at about 607 and 660 nm, respectively. The Q band peaks of

ZnTPP and ZnTAPP, however, were spectrally shifted, which may be due changes in aggregation, such as formation of a different aggregate type (i.e. H- versus J-aggregate). Fluorescence intensity ratios for the Q(0-1) to Q(0-0) peak were 1:1 for all porphyrins, with the exception of ZnTAPP, which had a 1:1.5 ratio.

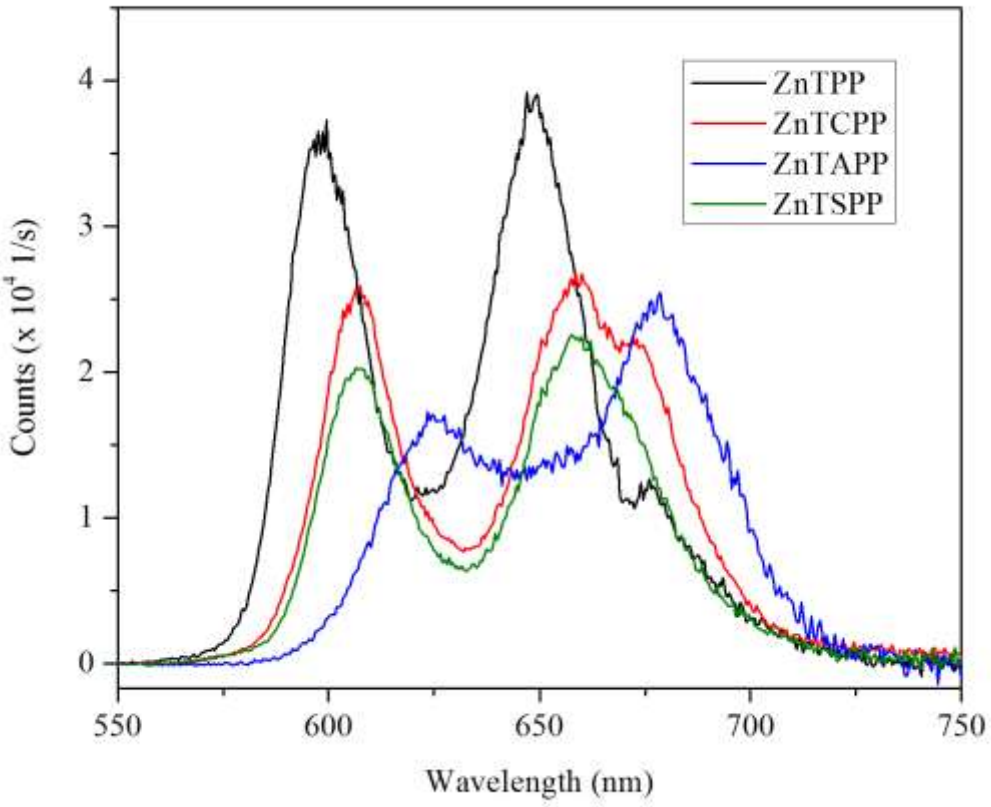

Figure 2.5 Corrected Q-band emission spectra of 200 μM Zn (II) porphyrins in different solvents (λ_{ex} = 532 nm). ZnTPP, ZnTAPP, ZnTSPP and ZnTCPP were dissolved in toluene, acetone, water, and methanol, respectively.

Despite having comparable absorbance to ZnTPP, ZnTCPP was found to have weaker upconverted fluorescence intensities in both the Soret and Q band regions. As seen in Figure 2.4, its Soret band was almost one hundred times weaker than that of ZnTPP, and its Q band emission was nearly half the intensity (Figure 2.5). However, compared to ZnTAPP and ZnTSPP, the carboxy-functionalized porphyrin was found to have a significantly stronger Soret band intensity (Figure 2.4). The large difference in fluorescence intensity found in the Soret region for the functionalized porphyrins may be due to any one of the solute and solvent interactions or to self-quenching as a result of increased aggregation.[13,42,49] Intensities of the Q bands were found to be comparable between porphyrins when the samples were degassed, and the Q band structures were also similar. This suggests that quenching of the upconverted S_2 emission was occurring.

The slight band broadening exhibited by ZnTAPP in Figure 2.5 further supported the previous speculation that this porphyrin aggregates more than ZnTCPP. Evidence of aggregation is often found in band broadening of absorbance spectra or spectral shifting in emission spectra.[4,5] Face-to-face stacking (H-aggregation) is known to result in significant blue-shifts of the spectra, along with fluorescence quenching.[5] Additionally, the Q(0-1) and Q(0-0) bands of ZnTAPP were significantly red-shifted from both ZnTPP (~25 and 31 nm, respectively) and the other functionalized porphyrins (~14 and 20 nm, respectively). Again, this is in agreement with the results obtained from the absorbance spectra, indicating that ZnTAPP undergoes more aggregation compared to the other porphyrins. The position of the Q band peaks of ZnTCPP (λ_{max} = 607 and 660 nm) and ZnTSPP (λ_{max} = 607 and 659 nm) are in close agreement. These peaks were also red shifted from the Q band peaks of ZnTPP (~7 and 12 nm, respectively),

indicating that aggregation concentration is also higher with the anionic porphyrins compared to ZnTPP.

Despite having weaker band intensities, the functionalized porphyrins exhibited spectral shifts that indicate occurrence of more aggregation, which is favourable for efficient upconversion by TTA to occur. Although having strong band intensity may seem more desirable, increased aggregate concentration may in fact introduce more opportunity for absorbance of emission by a neighbouring aggregate, resulting in self-quenching. These results were positive, as they were in agreement with results published in literature, where functionalized porphyrins are preferred as porphyrin sensitizers for DSSCs over free-base (without metal centre) or ligand-free porphyrins. Additionally, confirmation of upconversion capabilities by the Zn (II) functionalized porphyrins used in these experiments warranted further investigation of their photophysical behaviour on semiconductors.

2.4 Conclusion

The use of ZnTPP as a model reference was useful in determining the ability of the functionalized porphyrins to aggregate, which is critical for TTA to occur. It was also confirmed that the functionalized porphyrins exhibited spectral bands, such as the Soret and Q bands, that are quite typical for this class of molecules. The steady-state measurements carried out to assess the spectral properties of ZnTPP and its functionalized porphyrins indicated the potential to use these molecules as sensitizers in DSSCs. This was indicated through the varying degrees of aggregation observed in spectral shifts and band broadening. Aggregation is required in order to properly evaluate the potential for upconversion to occur. The impact that upconversion could have on energy conversion efficiencies in DSSCs is thought to be significant. This process is

achieved by absorbing a lower energy photon that will result in an excited electron that possesses more energy than the photon that was initially absorbed. Capabilities to undergo upconversion could be potentially useful in applications towards DSSCs, which will be further discussed in a later chapter.

Chapter 3: Spectroscopic Properties of Metalloporphyrins on TiO_2 Thin Films

3.1 Overview

To evaluate the potential of the Zn (II) porphyrins as sensitizers for DSSC applications, the spectroscopic properties of TiO_2 porphyrin-sensitized thin films were studied. Steady-state absorption and fluorescence measurements were carried out to determine the photophysical behaviour of the porphyrins adsorbed on a solid state film, and results were compared to those obtained from solution-based measurements presented in Chapter 2. Most importantly, the upconverted fluorescence of the sensitized thin films was also measured to determine if the porphyrins were capable of undergoing TTA. The results from these particular measurements were significant in determining the potential of using upconversion techniques in DSSCs. These measurements also highlighted the importance of the functional group as a linker to the semiconductor surface. The steady-state measurements and upconverted emission results of the porphyrin-sensitized thin films are presented and discussed in this chapter.

3.2 Materials and Methods

Chemicals

All chemicals and solvents were used without further purification. Titanium (IV) ethoxide (technical grade and purum) and poly(ethylene glycol)-*block*-poly(propylene glycol)-*block*-poly(ethylene glycol) (M_n 5800) (P123) were obtained from Sigma-Aldrich. Poly(methyl methacrylate) (MW 75000, 200 μm beads) (PMMA) was obtained from Polysciences, Inc. All solvents used (ACS grade) were purchased from EM Science (toluene), VWR (methanol), EMD (hydrochloric acid (36-38.5%), and Commercial Alcohols (100% ethanol, [EtOH]). Millipore water (resistivity 18.6 MΩ·cm) was used from a Milli-Q purification system.

Sample Preparation

Synthesis of mesoporous TiO_2 films followed the procedures described by Agarwala *et al*[50] and Zukalová *et al*[32]. The TiO_2 precursor solution was prepared by first adding 90 µL concentrated HCl (~1 mmol) dropwise to 1 g technical grade titanium ethoxide (~4 mmol) under vigorous stirring. Following slow addition of acid, 8 mL of P123 block co-polymer solution (~8 mM) was added. This polymer solution was prepared by adding 38 mL EtOH to 1.8 g of P123 (~0.3 mmol). The resulting precursor solution was allowed to stir overnight, and then aged in the refrigerator for 2 days.

The precursor solution (100 µL) was spincast onto a clean glass substrate (18 mm x 18 mm, No. 1 thickness, VWR) at 1000 rpm for 60 seconds using a spincaster (WS-400A-6NPP, Laurell Technologies Corporation). Prior to spincoating, the substrate was sonicated (Branson 1510 Ultrasonic Cleaner, VWR) in MeOH for 5 minutes, rinsed with EtOH, and then dried with nitrogen. Following this, the glass slides were place in a plasma cleaner (Plasma Cleaner PDC-32G, Harrick Plasma) for 20 minutes. The spincast substrate was aged for 2 days before calcining in a tube furnace (Lindberg/Blue Tube Furnace). The sample was calcined by heating up to 400°C (rate = 1°C/min), followed by a dwell period of 4 hrs at this temperature before being allowed to cool naturally down to room temperature.

Titania thin films were sensitized with 1 mM porphyrin solutions via spincasting or dropcasting. With the spincasting method, samples were sensitized with 20 layers of 1 mM porphyrin solution (120 µL aliquots) at 1000 rpm for 60 seconds. Each layer was added individually. Dropcast samples were prepared with 10 layers of 1 mM porphyrin solutions (120 µL aliquots), with each layer allowed time for drying through evaporation. PMMA thin films were prepared by spincoating clean glass slides with 150 µL PMMA solution (2% by mass) at

1000 rpm for 60 seconds. Sensitization of PMMA thin films was carried out using the same preparation methods as described for the titania thin films.

Instrumentation

Absorption spectra were recorded with a Varian Cary 500 Scan UV-Vis-NIR spectrophotometer using 10 mm x 10 mm cuvettes. Fluorescence spectra were recorded with a Photon Technology International spectrofluorometer using a CW 532 nm Nd:YAG laser as the excitation source. All fluorescence measurements were carried out by securing the sample to a solid state sample holder, which was attached to a vacuum line pumping down the sample. Upconverted fluorescence measurements were collected in the ranges of 400 – 500 nm (for the B band) and 550 – 750 nm (for the Q band). The illuminating power of the laser was controlled using an optical density filter prior to the beam hitting the sample, and a notch filter was used to remove scattered laser light. Excitation power at the sample was measured to be ~3.5 mW. Absorption spectra were collected in the 350 – 700 nm range. All measurements were carried out at room temperature.

Characterization of TiO_2 thin films

UV-Vis absorption spectroscopy (Cary 500 Scan UV-Vis-NIR Spectrophotometer, Varian Inc.) was used to verify that TiO_2 had been synthesized. The presence of mesopores was determined by using atomic force microscopy (AFM; Dimension Hybrid Nanoscope system, Veeco Metrology Group) and transmission electron microscopy (TEM) imaging (Philips CM10). A rough estimate of average pore size was determined through use of TEM. Morphology of the TiO_2 films was investigated using AFM (contact mode, 1.0 Hz scan rate, height trace).

3.3 Results and Discussion

3.3.1 Preparation and characterization of TiO_2 thin films

The degree of order of the mesoporous TiO_2 framework has previously been found to increase efficiency of solar cells.[1,22,51-53] A mesoporous structure increases surface area allowing for greater amounts of sensitizer to be adsorbed. The presence of pores in the titania films prepared here were verified using AFM imaging, where distances between particles can be observed (Figure 3.1). Pore sizes, however, were not determined, as this is typically done so through porosity measurements using adsorption techniques. TEM imaging was used to determine the size of the TiO_2 nanoparticles (~9 nm) (Figure 3.2). Sample preparation and TEM imaging was carried out using finely ground TiO_2 that was scraped off a glass slide. Particle size was estimated to be ~9 nm; however, the concentration of the nanoparticles was quite high, and because of this, accurate determination of particle size was difficult.

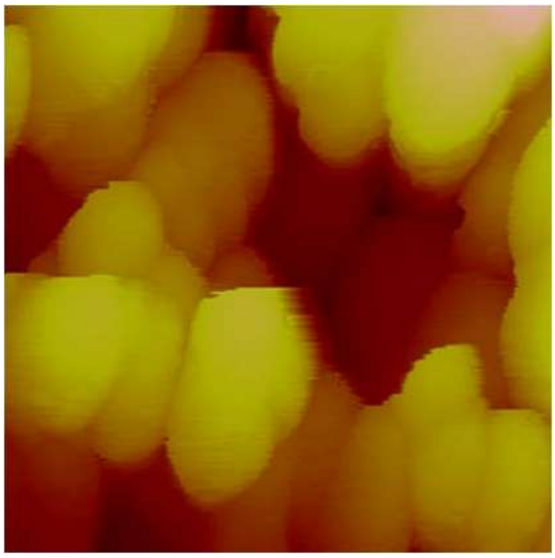

Figure 3.1 AFM height image of calcined TiO_2 thin film on glass showing titania particles (image size ~270 nm x 270 nm).

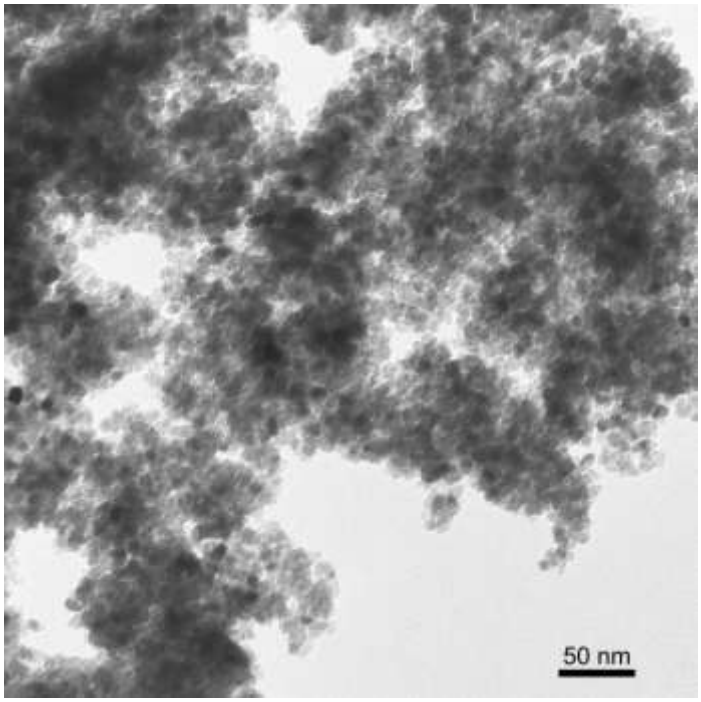

Figure 3.2 TEM image of mesoporous TiO_2 (sample magnification 110 000 x).

The absorption spectrum for the TiO_2 films (Figure 3.3) consisted of a single, well defined peak, with a maximum absorbance at ~290 nm. The single peak observed in the absorption spectrum is characteristic of TiO_2 and corresponds to the energy band gap between the valence band and conduction band.[54,55] Optical properties of spincast titania films are known to be influenced by both the pore size and pore density. The calculated experimental band gap (3.27 ± 0.04 eV) agrees quite well with the literature value of 3.2 eV.[56]

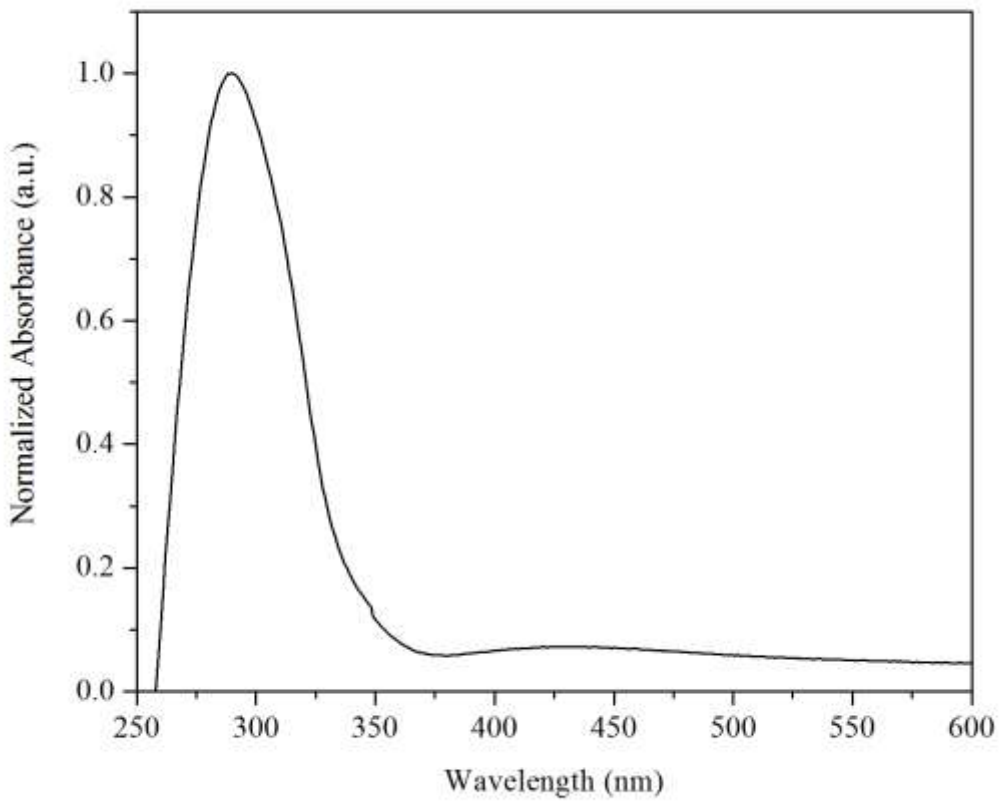

Figure 3.3 Normalized absorbance spectrum of mesoporous TiO_2 thin film.

3.3.2 Optical spectroscopy measurements

Once the successful synthesis of mesoporous TiO_2 was confirmed, absorbance and fluorescence spectra were recorded for the porphyrin-sensitized samples. The spectra collected for the solid-state samples differed from those of the solution-based measurements, possibly due to decreased aggregate concentration and interaction of the porphyrin with the titania. The surface concentration of each porphyrin is expected to vary between samples due differences in

the affinity of the porphyrin linker group with the Ti^{4+} center. The functional groups play a vital role in linking the porphyrin to the titania surface, in addition to affecting porphyrin aggregation.

This will ultimately affect the porphyrin's ability to undergo upconversion. For example, a carboxyl group will interact with the titania framework differently than an amine group as these two functional groups form different bonds with different bond strengths. It was expected that anionic linker groups would form stronger bonds with the positively charged titanium centre. Of the two anionic porphyrins, ZnTCPP was expected to have the strongest absorbance, since this was the trend observed in solution. In Chapter 2, ZnTAPP was observed to have the weakest absorbance out of all the Zn (II) porphyrins, and was predicted to again exhibit the weakest absorbance on titania.

Figure 3.4 shows the absorbance spectra of the various porphyrins adsorbed on the mesoporous TiO_2 thin films. Each absorbance spectrum shows the characteristic TiO_2 absorbance band at around 300 nm, which had a stronger intensity compared to the porphyrin absorbance bands. The Soret bands of the porphyrins appeared in the range of 400-450 nm as single peaks, with the exception of ZnTCPP which appeared as a split peak. The Q bands appeared between 525-650 nm, but the double peaks were relatively weak compared to solution measurements. The Q bands were also broadened in comparison to solution measurements; the ZnTPP and ZnTSPP Q bands were unclear due to band broadening and weak intensity.

ZnTCPP displayed the strongest absorbance, which was expected given that it was the strongest absorber of the ZnTPP derivatives in solution. Surprisingly, ZnTAPP has a stronger absorbance than ZnTPP, which was not observed in the solution-based measurements. This could also be attributed to more favourable interaction between ZnTAPP and titania, wherein the

lone pair of the amine is resulting in the amine group behaving similarly to ZnTCPP. The anionic-substituted porphyrins were predicted to have greater dye loading since these linker groups would interact most strongly with the titania. Although this was the case for ZnTCPP, ZnTSPP was found to exhibit the weakest signal overall. ZnTPP was predicted to have the weakest signal considering it has no linker group, resulting in the lowest dye loading. These results suggested that dye loading of ZnTSPP is lower than that of ZnTPP, possibly due to the forces of repulsion between neighbouring porphyrins being greater than the interaction with titania.

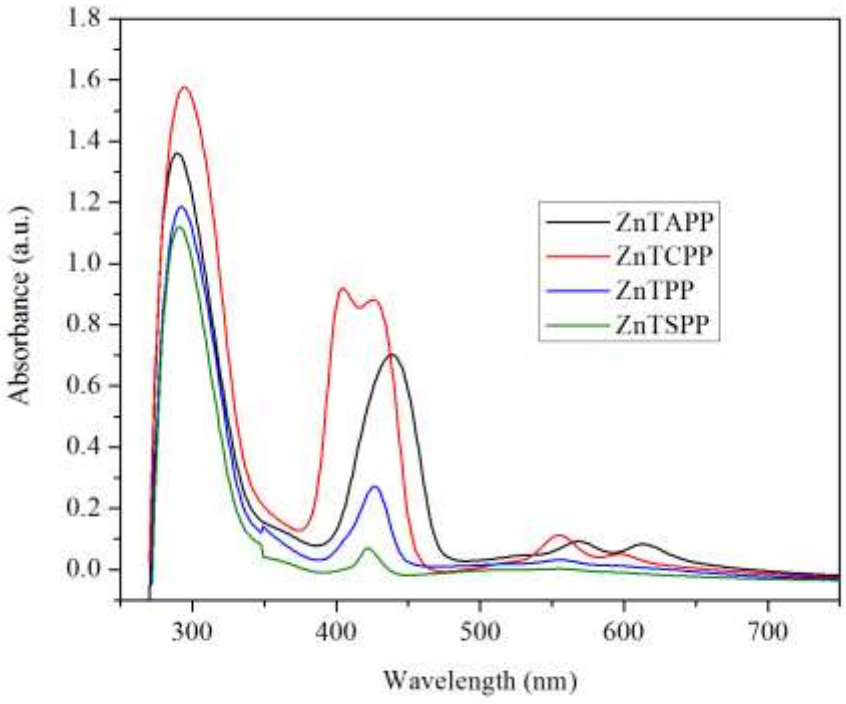

Figure 3.4 Absorbance spectrum of TiO_2 thin films sensitized with 1 mM porphyrin solutions.

Compared to the solution-based measurements, some spectral shifting in the Soret band positions was observed for the porphyrins adsorbed onto titania. The Soret band of ZnTCPP was observed to undergo splitting into two peaks (λ_{max} = 605 and 626 nm) and was also significantly blue-shifted by about 13 nm. Conversely, the bands for ZnTAPP and ZnTPP were red-shifted by 8 and 4 nm, respectively. The Soret peak position of ZnTSPP was comparable with its solution-based counterpart (λ_{max} = 422 nm). The spectral shifting observed may possibly be due to an increase in aggregation, or a change in orientation of the porphyrin, with respect to the titania surface, that affects saturation of the framework.[41,43]

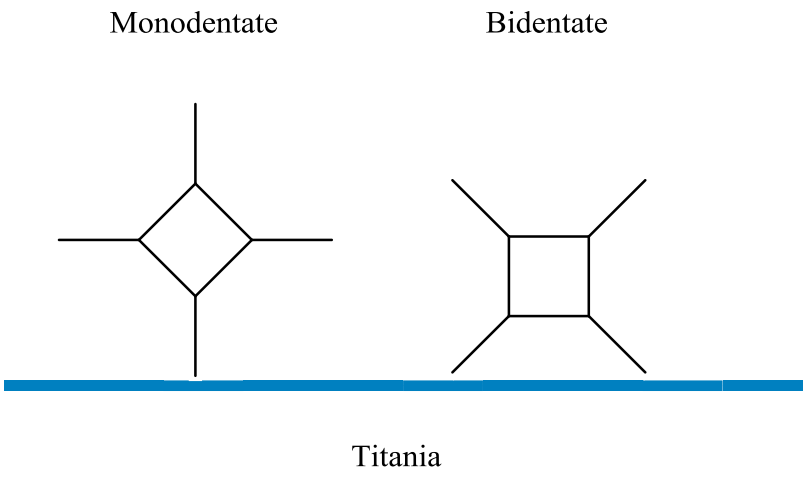

Figure 3.5 Illustration of two possible binding modes for the functionalized porphyrins.

In other words, the porphyrin could orientate itself either perpendicular to the surface by binding through one or two linker groups, or parallel to the surface, resulting in all four linker groups coming into contact with the surface. Monodentate binding, however, may result in the molecule tilting to assume an orientation that is more parallel.[39] For example, the possibility for

ZnTCPP to bind in either a mono- or bidentate fashion (Figure 3.5) with titania will affect the orientation of the porphyrin on the surface, which will in turn affect how the porphyrin aggregates in the film.[39,41] Kira *et al.* determined that bidentate binding led to a more densely packed dye monolayer on the titania surface, whereas monodentate bound porphyrins resulted in a loosely packed monolayer.[39]

Interaction with the adsorption surface is also influenced by the molecular structure of the dye and its linking group. For example, the carboxyl group has been reported in literature to interact with titania through either the metal centre or by forming hydrogen bonds with surface hydroxyl groups (Figure 3.6). The formation of aggregates is crucial for evaluating the impact that TTA could have on DSSC efficiencies. Although, ZnTSPP also possesses an anionic linker group, no significant spectral shift was observed. ZnTSPP was also found to have the weakest absorbance (Figure 3.4), which could be the result of poor deposition leading to a lower surface concentration.

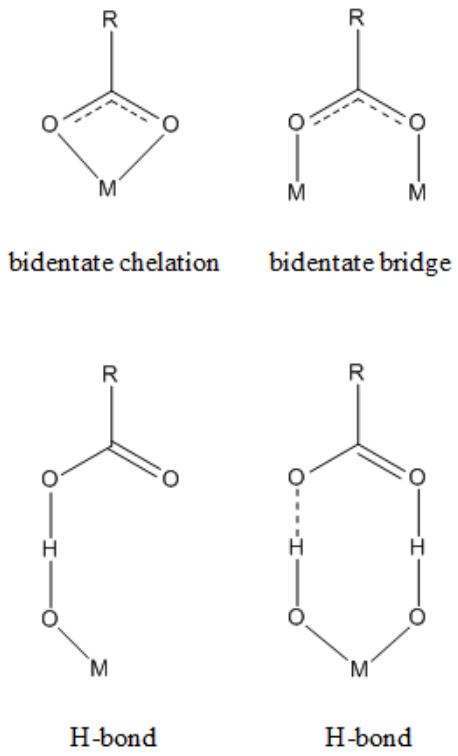

Figure 3.6 Illustration of the different possible binding modes a carboxyl group can establish with TiO_2, where M is the metal centre.[26]

The normalized upconverted S_2 emission spectra of the sensitized TiO_2 thin films are shown in Figure 3.7. The S_2 band appeared as a single peak within the range of 330–345 nm. While Figure 3.4 showed that ZnTSPP was observed to have the weakest absorption in the S_2 region, it was observed to have the strongest S_2 emission, with a relative intensity of ca. 1.5 x that of other porphyrins. ZnTAPP, ZnTCPP, and ZnTPP were found to have comparable S_2 emission intensities.

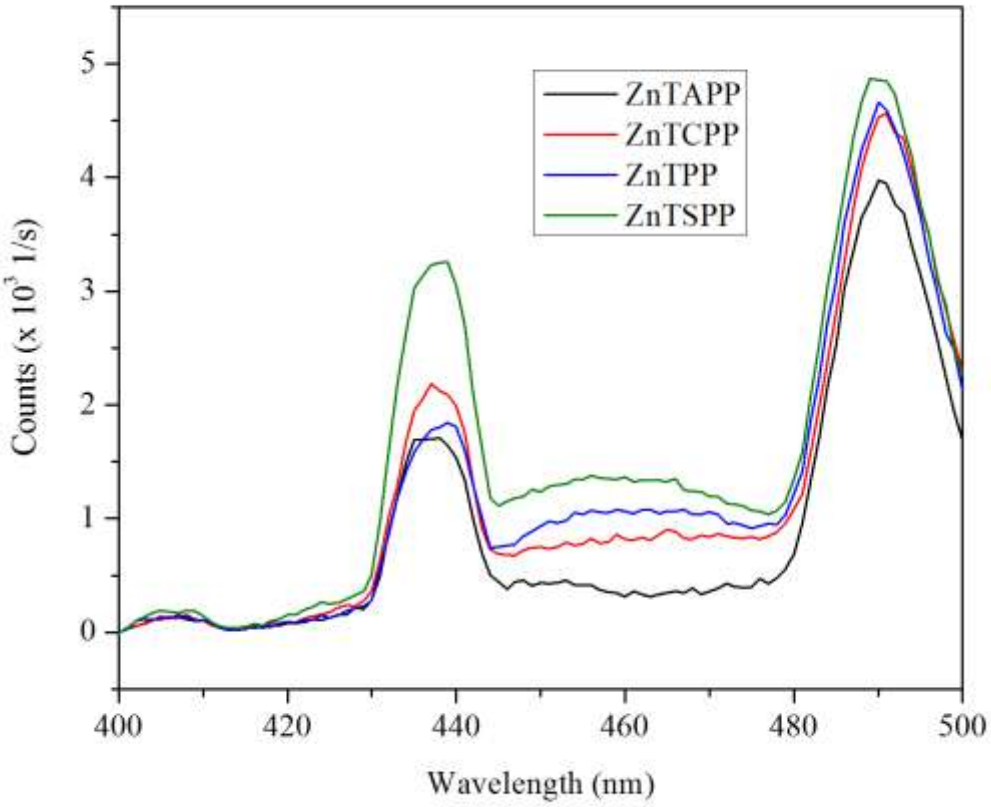

Figure 3.7 Normalized upconverted S_2 emission spectra of TiO_2 thin films spincast with 1 mM porphyrin solutions (λ_{ex} = 532 nm).

Despite the numerous studies of porphyrins found in literature, upconverted fluorescence of porphyrins on semiconductor materials has only recently garnered substantial interest. The measurement of upconverted fluorescence is important because it demonstrates the possibility of using photon upconversion to achieve higher photon conversion efficiencies. If upconversion can be harnessed as a means for improving DSSCs, then it has the potential to revolutionize this area of photovoltaic research and development. In view of that, the upconverted emission data

obtained for these porphyrin/TiO_2 systems are significant preliminary results, in addition to being a novel discovery.

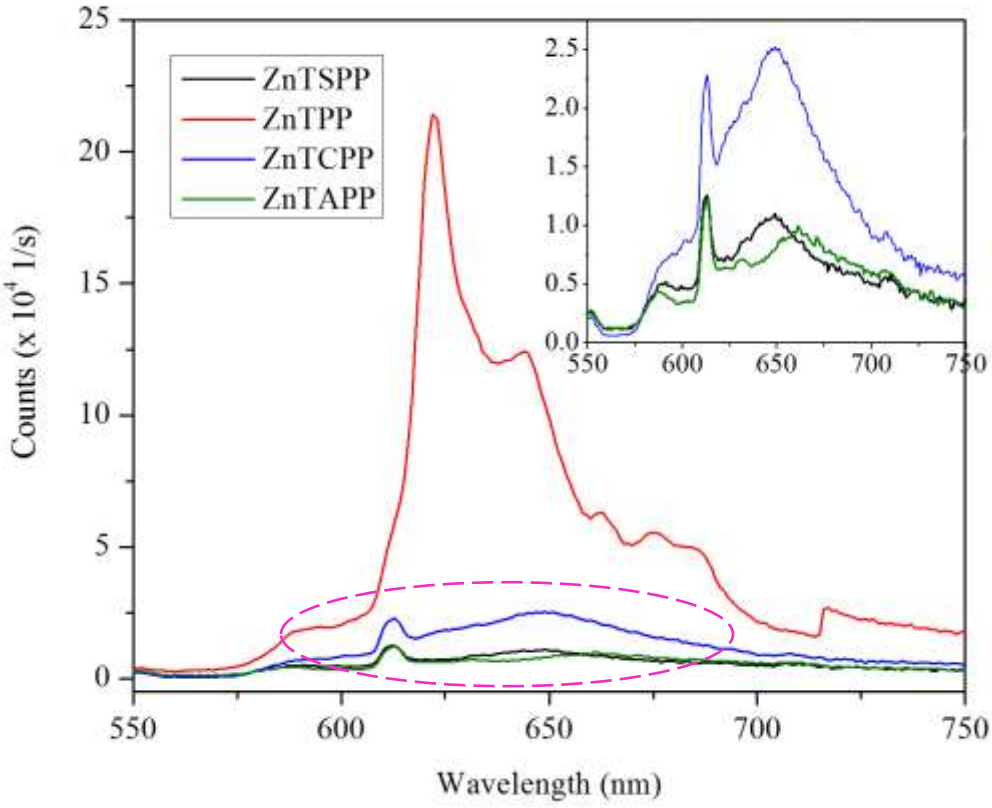

Figure 3.8 Normalized Q band emission spectra of TiO_2 thin films spincast with 1 mM porphyrin solutions (λ_{ex} = 532 nm) (inset shows an enlarged image of the circled area).

The normalized Q band emission spectra of the porphyrin-sensitized titania thin films is shown in Figure 3.8. The significant difference in the Q band emission observed from the porphyrins on TiO_2 is apparent. Emission scans were collected of blank TiO_2 thin film in the Soret and Q band region. Absence of any significant signal in these spectra indicated that TiO_2 did not contribute significantly to the fluorescence of the porphyrin/titania systems. There was a

large difference observed in the relative intensities between ZnTPP and the functionalized porphyrins.

The Q bands appeared as a single, broad peak within the 575–750 nm range, with some small features observed on the band. All porphyrin spectra were lacking several characteristic structures which were observed in the emission spectra of the solution-based results. The absence of distinct Q(0-0) and Q(0-1) transition peaks is seen more clearly in the inset of Figure 3.8. This broad peak appears around 650 nm. A sharp peak is also observed at 613 nm (see inset of Figure 3.8), possessing emission intensities that are similar in all three of the functionalized porphyrins. The emission peak is too sharp to be attributed to a molecular species, and is likely due to scattering.

ZnTCPP was found to have a stronger Q band emission in comparison with ZnTSPP and ZnTAPP. Although the Q band peak for ZnTCPP and ZnTSPP is observed at the same position (λ_{max} = 649 nm), a red-shift (12 nm, λ_{max} = 661 nm) from this wavelength is observed for ZnTAPP. This may simply be due to a change in aggregation of the porphyrins due to limitations of binding modes of the different functional groups. Broadening and convergence (appearance of a single peak, rather than two) of the emission peaks is also indicative of the formation of H-aggregates.[38]

Additional structures that were apparent in the emission spectra were the peaks found near 490 nm (Figure 3.7) and a portion of another is displayed clearly in the inset of Figure 3.8. These peaks were possible due to impurities present in the porphyrin samples, such as chlorins. When one of the β-β double bonds found in porphyrins is reduced, the result is the formation of a chlorin, a porphyrin derivative, making it a common impurity found in porphyrin samples.[14]

Although loss of the double bond does not disrupt delocalization of the macrocycle, the emission spectrum is markedly different from that of a porphyrin. The Q band spectra of the free-base chlorin shows four distinct peaks.[14] The spectra shows a band of weak intensity centered at ~500 nm, a peak of weaker intensity between ~530–540 nm, followed by another weak peak at ~600, and a strong sharp peak at ~650 nm. This sharp peak has an intensity that is about 5 x greater than the peak that appears at ~500 nm.[14] The additional peaks observed in the emission spectra coincide closely to the emission peaks found in chlorins. The intensity of these peaks may appear stronger due to the very weak upconverted emission detected from the Zn (II) porphyrins, which may be due to electron injection from the Zn (II) porphyrins into the titania conduction band limiting the amount of excited electrons available to fluoresce from the S_2 state.

To determine the possible nature of the interaction between the TiO_2 semiconductor and porphyrin, the Q band emission of mixed PMMA–porphyrin films was measured. ZnTPP in a film of the polymer PMMA was chosen as a control because upconversion has previously been studied with this system.[4,5] Figure 3.9 compares the S_1 fluorescence of the PMMA/ZnTPP and TiO_2/ZnTPP system. The S_1 emission of the semiconductor system shows a distinct peak, whereas the polymer system is a broadened band. It should be noted that PMMA is expected to be amorphous, making comparisons with titania weak. A comparison of the Soret band was not possible, due to unsuccessful attempts at measuring the weak emission in this region.

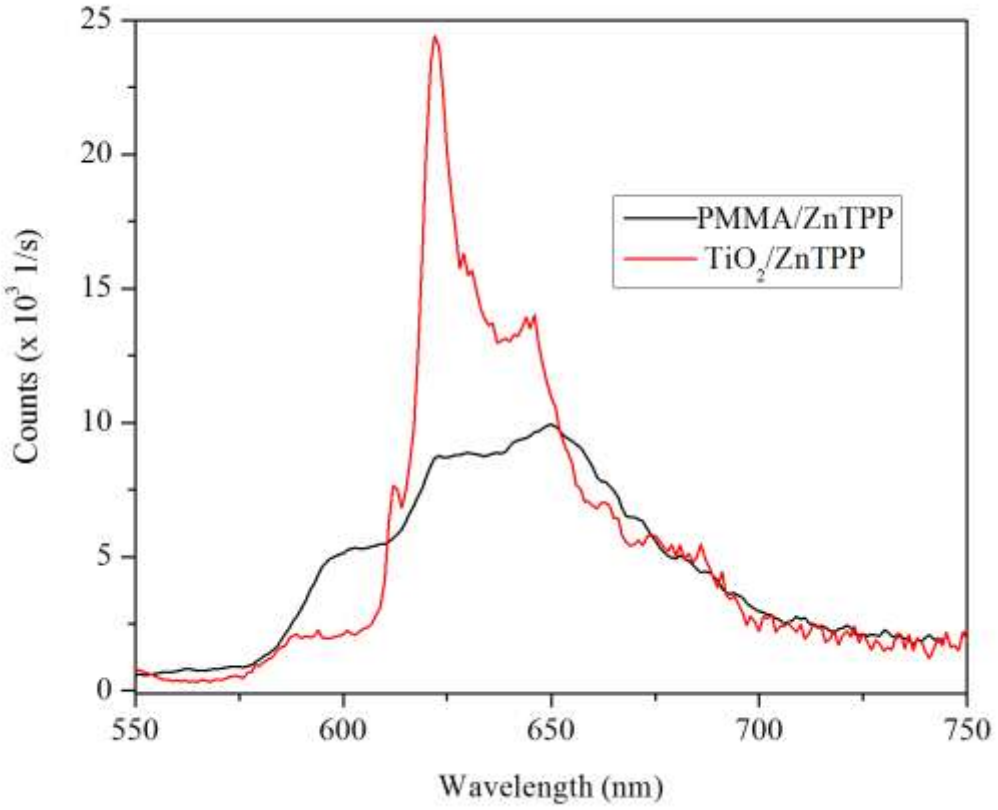

Figure 3.9 Fluorescence spectrum comparing S_1 emission of TiO_2 and PMMA films spincast with 20 layers of 1 mM ZnTPP.

The relative intensity measured for the S_1 emission of the ZnTPP/PMMA system was half of that measured for the ZnTPP/TiO_2 sample. The PMMA system was also found to lack the emission structure found in the TiO_2/ZnTPP emission. A convergence of the Q(0,0) and Q(0,1) peaks was observed as a general broadening within this region. These changes in the Q band structure may be due to the different morphology of each media, since this will affect the amount of ZnTPP adsorbed onto each sample as well as the orientation of the macrocycle.

It would be expected that the amount of ZnTPP loading onto TiO_2 would be higher compared to the PMMA sample because of its mesoporous matrix, possibly aiding in the formation of more organized aggregates. This may be why two distinct peaks are observed for this system. The broadening observed for the PMMA/ZnTPP system suggests the formation of random aggregates. Unfortunately, this does little to clarify the effect that the interaction of TiO_2 with the various porphyrin functional groups has on the optical properties of the system.

Figure 3.10 shows the S_1 fluorescence observed in the PMMA systems sensitized with ZnTPP and ZnTCPP. The emission spectrum for the ZnTPP/PMMA system consisted of two broadened peaks ($\lambda_{0\text{-}0}$ = 629 nm and 647 nm, $\lambda_{0\text{-}1}$ = 668 nm and 681 nm). The relative intensity of the Q(0-1) band was close to half that of Q(0-0). Unlike the ZnTPP system, ZnTCPP appeared as a single broad peak with a very weak relative intensity. The Q band spectra for ZnTPP/PMMA system found in literature, on the other hand, showed a single defined Q(0-1) peak at ~640 nm that was double the intensity of the Q(0-0) band (~600 nm).[4] The Q band spectra reported in literature was collected using samples prepared with 1 μM porphyrin solution, a significantly lower concentration than that used in these measurements. An increased concentration will increase the porphyrin population returning to any of the vibrational energy levels found in the ground state. This tends to manifest in the spectra as broadening.

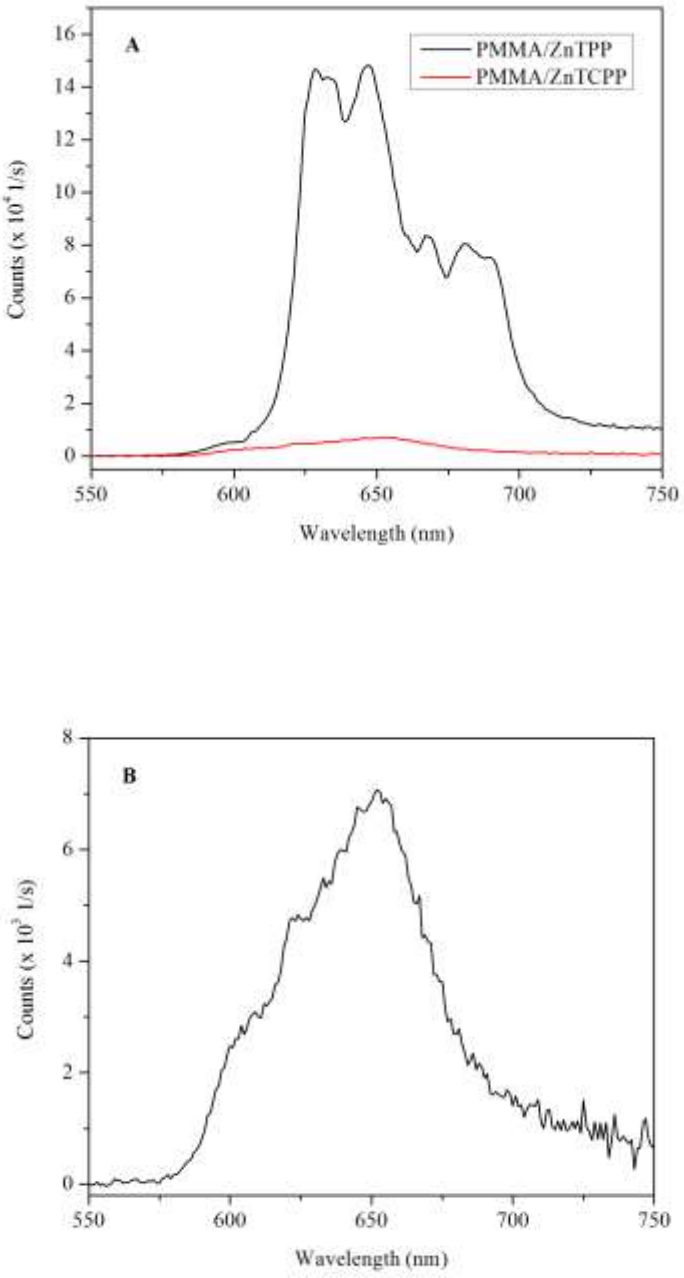

Figure 3.10 Fluorescence spectra of PMMA films dropcast with 10 layers of 1 mM porphyrin solutions excited at 532 nm. The S_1 emission of ZnTPP is compared with that of ZnTCPP (A). The S_1 emission of ZnTCPP is shown more clearly (B).

These films were prepared through the use of dropcasting rather than spincasting in order to prepare samples that were more concentrated. Spincast samples were prepared by spincasting the film at 1000 rpm for 1 minute following each drop. Dropcast samples were prepared by allowing solvent to evaporate between each drop, promoting increased surface concentration. In doing so, however, the dropcast method was found to yield an S_1 emission spectrum that differed significantly from the system prepared through use of spincasting (Figure 3.9). With the dropcast method, a general structure of two Q band peaks was observed which was absent from the spincast PMMA/ZnTPP system. This suggests that dropcasting allows the porphyrins sufficient time to self-assemble into more organized aggregates, similar to those potentially found within the titania framework.

The PMMA/ZnTCPP system was found to have a much lower Q band emission intensity than that of the ZnTPP system (Figure 3.10). Additionally, the PMMA/ZnTCPP system exhibited band broadening, as well as the presence of the Q bands as a single peak (λ_{max} = 652 nm). This single Q band peak is comparable to the peak observed for the titania/ZnTCPP system, suggesting the possibility that the aggregates formed are similar in orientation and type. Moreover, the Q band emission of the sensitized TiO_2 samples also exhibited similar differences in intensities between ZnTPP and ZnTCPP.

Absorbance spectra comparing the PMMA films sensitized with ZnTPP via spincasting and dropcasting are shown in Figure 3.11. Both samples had a strong absorbance band in the Soret region, and two broadened peaks of weaker relative intensity in the Q band region. The spincast system had a weaker relative intensity compared to the dropcast sample, which is more evident in the Soret band. The spincast system was also found to be red-shifted from the dropcast system (10 nm, λ_{max} = 435 nm). This suggests variations in both the types and

concentration of different aggregates formed in the samples. Different methods of thin film sensitization may affect how the macrocycles aggregate, which in turn will affect the optical properties observed for each system. Additionally, the concentration of porphyrin across the sample may not be uniform.

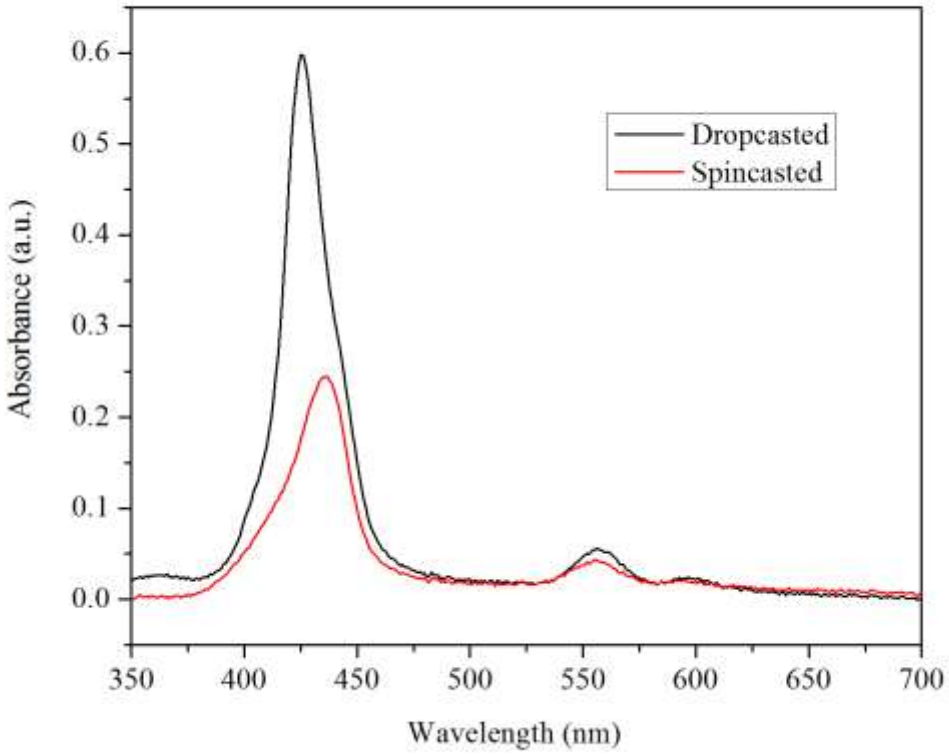

Figure 3.11 Absorbance spectra of PMMA films comparing sensitization with 1 mM ZnTPP by dropcast (10 layers) and spincast (20 layers) methods.

The results of these measurements prompted investigation into the degree of dye loading into the TiO_2 framework. Since each porphyrin is expected to interact differently with the TiO_2, it was deemed necessary to determine the amount of time needed to saturate the thin films with dye through dip-coating of each porphyrin. In this experiment only ZnTPP was investigated and it was assumed that the anionic nature of the functionalized porphyrins used in this study would have a higher affinity for the Ti^{4+} center.

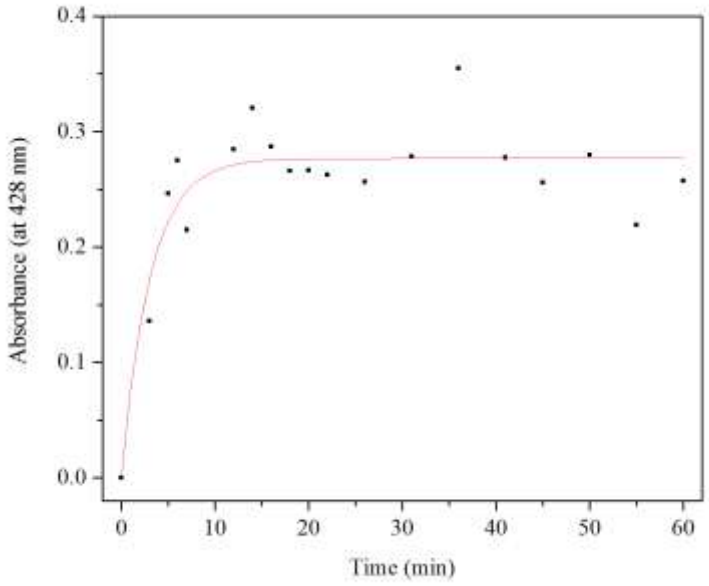

Figure 3.12 Absorbance measurements at 428 nm for a TiO_2 thin film allowed to soak in 1 mM ZnTPP solution for varying lengths of time. The red line represents the saturation curve, serving as an indicator for film saturation.

Figure 3.12 shows an example of a saturation curve, which was obtained by soaking a TiO_2 thin film in a 1 mM ZnTPP solution for different lengths of time up to a maximum of one hour. The absorbance intensities measured at 428 nm (Soret absorbance peak) was collected for

the varying lengths of soaking times. These measurements indicated that the film reached saturation at about 10 minutes, and further soaking did not have a significant impact on dye loading. This was necessary to determine how the length of soaking the film affected dye loading.

Despite efforts made to achieve a uniform monolayer of porphyrin on the titania, the precise structure of each titania film was a factor that was difficult to control. The differences in emission and absorption observed between solution- and titania-based samples are an indicator of some of the complexities that might be expected when developing photovoltaic devices. In particular, the processes of electron injection and charge transport into an external circuit greatly affect the performance of the device, which involves both the semiconductor and sensitizer.[26] Numerous studies have shown that film thickness and porosity greatly affect charge transport, presenting some problems when trying to study photophysical behaviour of sensitizers on semiconductors.[20,26,29,32,33,38,41,50]

Orientation of the fluorophore with respect to the semiconductor affects electron transfer by influencing the distance between donor and acceptor.[2] Rochford *et al.* investigated the different orientations (ie. monodentate or bidentate) that ZnTCPP assumes when binding to ZrO. They observed a blue shift for their ZnTCPP/ZrO system and associated this with the formation of H-aggregates (face-to-face molecular stacks). Deposition onto titania influenced how the porphyrin interacted with its surrounding environment by affecting its orientation.[26] Since the porphyrin is no longer in solution, the rates of diffusion that would be expected to influence its optical properties no longer apply, and as a result the electron-transfer rates (charge injection into the semiconductor conduction band, or excited state decay of the dye) may also be affected.[26]

Electron injection into the semiconductor is believed to occur on the femtosecond time-scale. The fast charge injection limits the electrons populating the excited states of the dye, thus affecting emission intensity.[26] It is known that linker groups improve electron transfer from the sensitizer to the semiconductor, aiding electron injection into the conduction band of the semiconductor.[19,39,43] Electron-rich functional groups are expected to establish a dipole-dipole interaction with the titania, limiting the distance between the dye and semiconductor. In the case of ZnTCPP, carboxyl-groups tend to bind very strongly to each other and the Ti^{4+} center. Similarly, the lone pair in the amino group of ZnTAPP should be able to facilitate an improved electron transfer rate compared to ZnTPP, which lacks an electron-rich functional group. This supposition was reinforced by the absorbances shown in Figure 3.4, where ZnTCPP and ZnTAPP exhibited the strongest Soret band absorbances.

3.4 Conclusion

Mesoporous titania thin films were prepared in order to determine how interaction with the semiconductor framework affects the optical properties of the porphyrin sensitizers, particularly the ability to undergo TTA. Steady-state absorbance and emission measurements were taken of the sensitized titania films. ZnTCPP was found to have the strongest absorbance, and of the functionalized porphyrins, it had the strongest Q band emission. Overall, ZnTPP had the strongest Q band emission.

The most significant result gathered in these experiments was the upconverted emission spectra for the porphyrin-sensitized titania thin-films. The strongest upconverted Soret band was observed with the ZnTSPP sample. Strong emission is indicative of high population of the excited states. The strong upconverted S_2 emission measured for ZnTSPP is an indicator of

weak charge injection into the semiconductor, especially considering it also had the weakest absorbance. Proper evaluation of upconversion was difficult due to possible effects that interactions between the porphyrin and TiO_2 have on electron transport within the system. Changes in the optical properties of porphyrins on titania versus solution-based results were indicative of some variables that would affect evaluation of a complete solar cell.

Chapter 4: Fabrication and Testing of DSSCs

4.1 Overview

Preliminary measurements to evaluate the effectiveness of the Zn (II) porphyrins as DSSC sensitizers were conducted. Current-voltage (*I-V*) response curves were measured for the photovoltaic cells, and the electrical power outputs of the cells were determined. The set-up used to measure the current was tested with anthocyanin-sensitized solar cells, a system typically used in classroom settings to teach the principles of solar cells. The data collected using the Zn (II) porphyrin systems are presented and discussed in this chapter. ZnTCPP was found to be the best sensitizer by producing the highest current densities and open-circuit voltages (J_{max} = 0.115 mA/cm^2, V_{oc} = 433 mV), which are the experimental values used to evaluate photon-to-current conversion efficiencies. The *I-V* curves were also a good indication of the affect that the linker groups have on the charge injection process. This coincides well with what was found in literature, where carboxyl groups are among the most commonly used linkers.

4.2 Materials and Methods

Chemicals

All chemicals and solvents were used without further purification. Titanium (IV) ethoxide (technical grade and purum) and poly(ethylene glycol)-*block*-poly(propylene glycol)-*block*-poly(ethylene glycol) (M_n 5800) (P123) were obtained from Sigma-Aldrich (USA). All solvents used (ACS grade) were purchased from EM Science (toluene), VWR (methanol), EMD (hydrochloric acid (36-38.5%)), and Commercial Alcohols (100% ethanol [EtOH]). The pre-made iodide electrolyte solution was obtained from a Nanocrystalline Solar Cell Kit from the

Institute for Chemical Education.[57] Millipore water (resistivity 18.6 MΩ·cm) was used from a Milli-Q purification system.

Cell Fabrication and Performance Characterization

Zn (II) porphyrin-sensitized solar cells were fabricated with a sensitized TiO_2/ fluorine-doped tin oxide (FTO) working electrode and carbon-coated FTO counter electrode. The working electrodes were prepared on 3.0 mm 8 Ω FTO-coated glass (Pilkington). TiO_2/FTO working electrodes were prepared by spincasting the TiO_2 precursor solution (~50–100 µL, dependent on size of glass) onto the FTO (1000 rpm, 1 min). FTO was cleaned using the same method to clean glass (see section 3.2). The electrodes were calcined in a tube furnace by allowing the temperature to rise from room temperature to 400 °C (rate = 1 °C/min) and holding at this temperature for 4 hours before cooling slowly back down to room temperature.

After calcination, the TiO_2 electrodes were immersed in 1 mM Zn (II) porphyrin solutions for an hour. Following soaking, the electrodes were rinsed with EtOH to remove porphyrins that were not adsorbed, and then dried with N_2. The carbon counter electrodes were prepared by lightly coating the FTO surface with graphite. The two electrodes were assembled into a cell, with care being taken not to rub off the carbon coating. An iodide electrolyte solution (0.5 M potassium iodide and 0.05 M iodine in dry ethylene glycol) was introduced between the two electrodes. Cells were illuminated using a halogen lamp (360 W).

Preliminary measurements on power conversion efficiency were determined by current-voltage curves. Two multimeters (Fluke 175 True RMS Multimeter; Fluke 77 Series II Multimeter) equipped with alligator clips, and a 10 kΩ variable resistor were used to collect the data. The circuit used is illustrated in Figure 4.1. The resistor was used to adjust the voltage,

and the resulting current was recorded. Figure 4.2 shows the set-up used to characterize and support the cell. Measurements of current were collected as the voltage was adjusted in steps of 10 mV from V_{max} to 0 V.

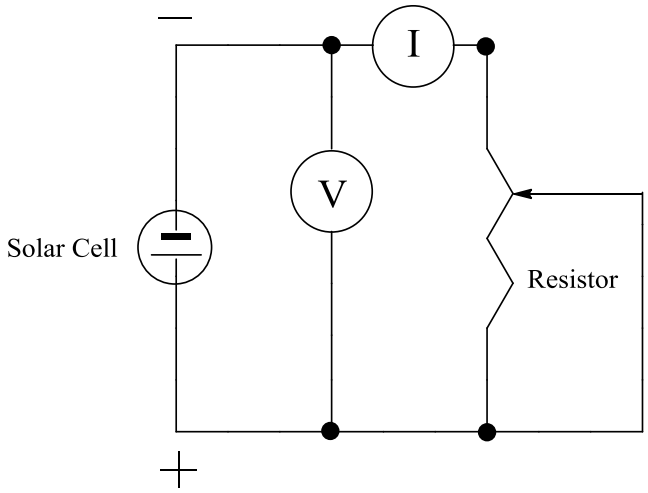

Figure 4.1 Circuit diagram used to measure current-voltage curves. One multimeter was used to measure current (I) and the other, voltage (V).

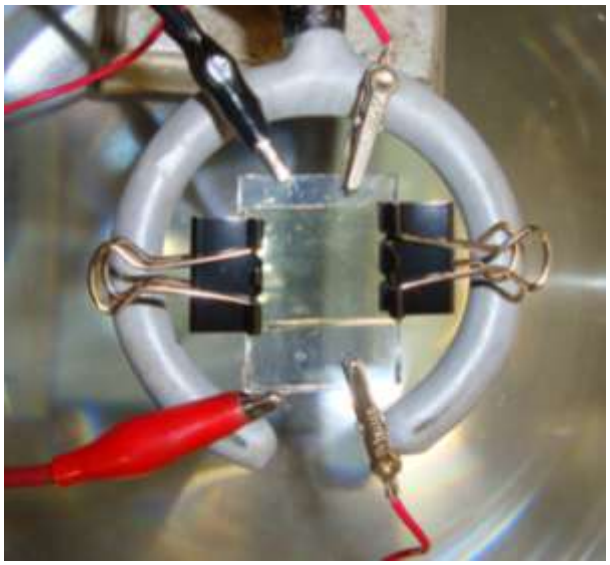

Figure 4.2 Photograph of a simple porphyrin-sensitized solar cell.

4.3 *I-V* curve measurements of porphyrin-sensitized solar cells

Absorption spectra of the Zn (II) porphyrins on TiO_2 were characterized by strong absorbances between 410 and 440 nm, which are characteristic of the porphyrin Soret band. The Q bands were characterized by lower intensity absorbance peaks between 550 and 615 nm. The Soret band peak intensities were used to assess the approximate concentration of porphyrins within the TiO_2 framework. These results are discussed in Chapter 3.

I-V curves provide useful information on the photon conversion efficiency of the DSSCs. Photon-to-current (ie. power) conversion efficiency is the typical value used to compare efficiencies of DSSCs. The power conversion efficiency (η) can be calculated by using the following equation[26]:

$$\eta = \frac{J_{sc}V_{oc}FF}{P_{in}} \qquad \text{(Eq 4.1)}$$

where J_{sc} is the short-circuit current density, V_{oc} is the open-circuit voltage, FF is the fill factor and P_{in} is the power density of the incident light. J_{sc} is the current measured when the voltage = 0 V. V_{oc} is the voltage measured when the current = 0 mA. The fill factor (FF) is a value ($0 < FF < 1$) that is used to indicate the shape of the *I-V* curve. These values are also discussed in the Introduction.

An ideal *I-V* curve will appear nearly rectangular in shape, indicating a higher efficiency of power conversion; that is, the maximum current density can be achieved more quickly. Such a curve will yield a FF value close to 1.[26] Degradation of the fill factor could be attributed to many factors relating to electron transport issues.[58] These problems can arise due to interfacial contact between the TiO_2/electrolyte and FTO/TiO_2 interface.[58,59] The thickness and framework structure of the TiO_2 contributes significantly to this as it directly affects the recombination pathway.[26,51,53,59]

The V_{oc} and J_{sc} are photovoltaic properties that indicate effects that the semiconductor has on the overall performance. V_{oc} and J_{sc} are important experimental values that are used to evaluate the performance of solar cells (see Equation 4.1).[30] They are good indicators of electron transfer efficiencies. It has been found that V_{oc} correlates with the energy band gap between the redox mediator and the semiconductor conduction band.[30] V_{oc} is influenced by the density and location of defects within the semiconductor, and the presence of impurities.[52] Studies have shown that with increasing titania film thickness, the V_{oc} decreases due to mass transport limitations and charge recombination resulting from the increased distance between interfaces.[1,39,53] J_{sc} measures the photocurrent that flows through the external circuit in the absence of a load.[30] It is limited by the rates of electron injection into the conduction band, regeneration of the sensitizer, and electron transport into the external circuit. Film thickness, in

addition to morphology, also affects J_{sc}, where it has been found to increase with increasing thickness.[52] Large V_{oc} and J_{sc} values are desired when engineering photovoltaics.

The preliminary current-voltage (*I-V*) curves collected from the porphyrin sensitized photovoltaic cells are presented in Figure 4.3. Table 4.1 lists results from measurements of individual DSSCs, as well as an indication of preparation reproducibility. The curves collected for the Zn (II) porphyrins are typical of *I-V* curves, which are characterized by slopes that plateau with a decreasing voltage. The gentle slopes depicted in the *I-V* curves offer a qualitative approximation for the low conversion efficiency of the cells assembled in this work. The y-axis intercept corresponds closely with short-circuit current density (J_{sc}) values, and is reported as maximum current (I_{max}) and current density (J_{max}) values in Table 4.1. The open-circuit voltages (V_{oc}) were recorded before attaching the resistor, and are also reported in Table 4.1. The V_{max} data points shown in the *I-V* curves are not the same as the V_{oc} values reported in the table.

The J_{max} and V_{oc} values measured for Zn (II) porphyrin systems are rather low compared to values reported in literature.[60,61] Reasonable comparisons can be made with other Zn (II) porphyrin systems, since porphyrins exhibit comparable spectra. Differences in intensities and spectral shifting can be attributed to functionalization at any of the outer positions of the macrocycle.[14,26] It should be noted that other factors that would affect DSSC performance are the choice of electrolyte and semiconductor.[30]

It was found that the ZnTCPP sensitized cell exhibited the strongest response with the largest maximum voltage (V_{max}) and maximum current density (J_{max}) at 260 mV and 0.115 mA/cm^2, respectively. The voltage response for this particular cell was able to go as low as 0.9 mV, resulting in a current density response from 0.019 to 0.115 mA/cm^2. The second best

performance measured was collected from the ZnTSPP sensitized cell, where the V_{max} was found to be 260 mV and J_{max} was 0.019 mA/cm^2 at 1.5 mV. The current density response for this cell was 0.010 to 0.019 mA/cm^2. A smaller voltage resulted in a smaller current density response for both ZnTPP and ZnTAPP sensitized cells. V_{max} values for ZnTPP and ZnTAPP were 161 and 28 mV, respectively, yielding responses from 0.006 to 0.009 mA/cm^2.

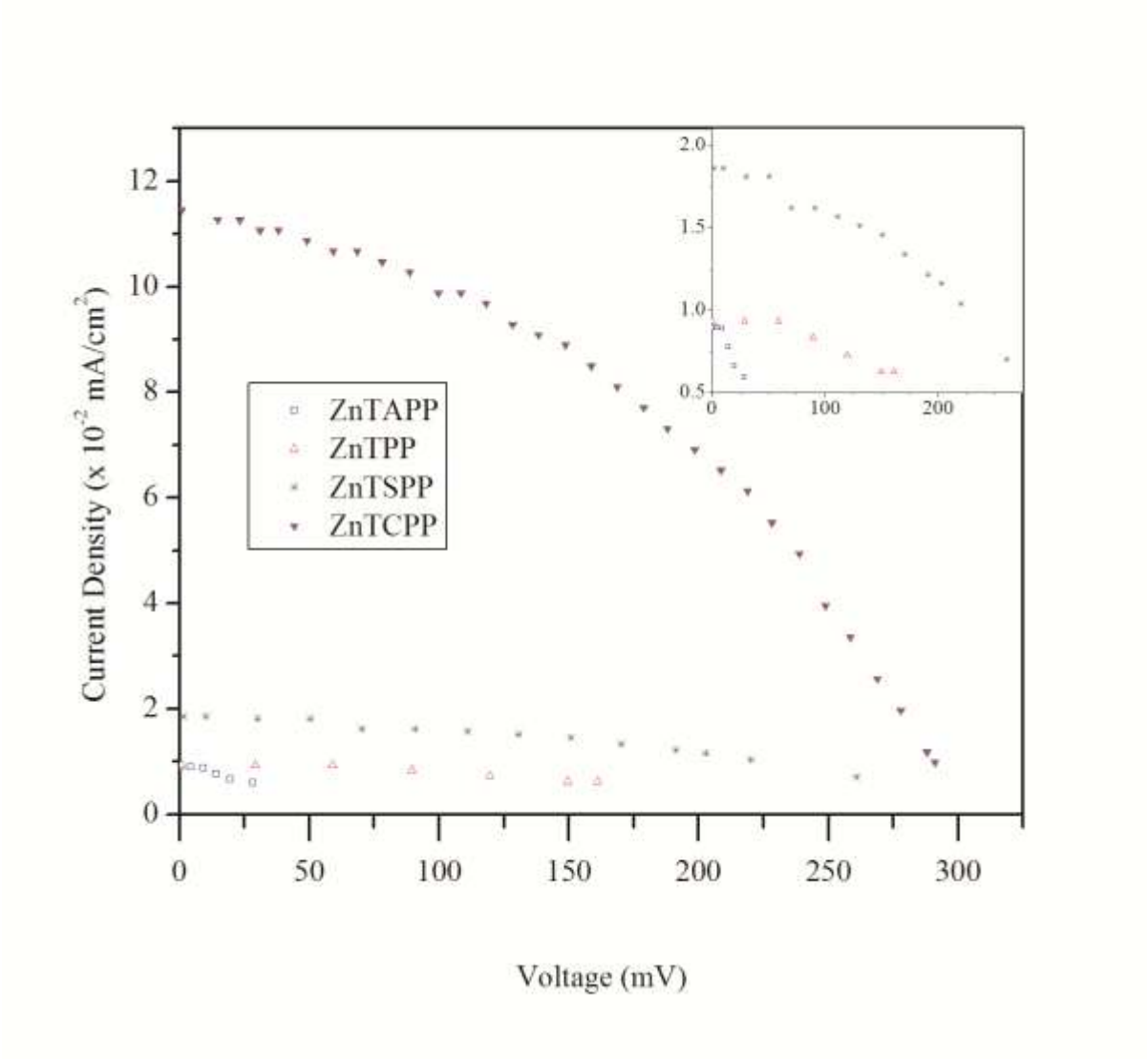

Figure 4.3 *I-V* curves of Zn (II) porphyrin sensitized solar cells (inset is a magnification of the lower intensity curves).

Using the photocurrent density and voltage values, the power density ($P = V \cdot I$) of each cell can be calculated. This allows for a more meaningful method for comparing the photovoltaic performance of each cell, especially since the power conversion efficiency, η, cannot be determined due to unknown power density of illumination (P_{in}). The calculated power densities of the cells are listed in Table 4.1. Table 4.2 displays the average power densities for each porphyrin sensitized solar cell, as well as the standard deviations.

Table 4.1 Photovoltaic parameters of Zn (II) porphyrin sensitized solar cells.

Porphyrin	V_{oc} (mV)	I_{max} (mA)	J_{max} (μA cm^{-2})	Power Density (mW cm^{-2})
ZnTPP	285	0.04	8	2.3
	240	0.05	11	2.6
ZnTAPP	39.9	0.06	14	0.54
	29.6	0.03	6	0.19
ZnTCPP	163	0.70	-	-
	67.4	0.42	83	5.6
	68.0	0.42	82	5.6
	133	0.44	85	11
	250	0.37	75	19
	433	0.29	66	28
	336	0.58	115	38
ZnTSPP	21.7	0.10	22	0.48
	308	0.11	24	7.4
	360	0.07	19	6.8

According to Table 4.2, the ZnTCPP sensitizer resulted in the largest power density (18 mW cm^{-2}), indicating a more efficient photon-to-current conversion compared to the other Zn (II) porphyrins. Considering carboxyl groups are a common ligand used in current DSSCs, the power density achieved in this study follows the trend of porphyrins with carboxyl groups found in literature, of which some values are mentioned below.[19,26,29,38,62] Although values achieved in literature are far greater (upwards to ~ 5000 mW/cm^2) than the power densities found in these experiments, the general notion is that carboxyl ligands play a key role in achieving high power densities and conversion efficiencies.[63,64]

Of the substituted Zn (II) porphyrins, ZnTCPP exhibited the strongest absorbance, both in solution and on titania. The ZnTAPP sensitized solar cell resulted in the poorest photovoltaic performance, with an average power density of 0.36 mW cm^{-2}. Although, ZnTAPP had comparable absorbance intensity to ZnTCPP, its S_2 and S_1 emission bands were the lowest intensity of the porphyrins indicating diminished population of states compared with the other porphyrins. ZnTSPP was expected to result in a larger current density than ZnTAPP due to its anionic nature, compared to the neutral amino group, despite achieving the weakest absorbance intensity on titania.

Table 4.2 Power density and standard deviation values for Zn (II) porphyrin sensitized solar cells.

Porphyrin	Number of Samples	Average Power Density (mW cm^{-2})
ZnTPP	2	2.5 ± 0.2
ZnTAPP	2	0.36 ± 0.25
ZnTCPP	6	18 ± 13
ZnTSPP	3	4.9 ± 3.8

The power densities reported in Table 4.2 are not as impressive as values in literature, but overall simplicity of the porphyrins used in this study may contribute to weak performance.[26] For example, Seo *et al.* reported DSSCs sensitized with 5, 10, 15-triphenyl-20-(4-carboxyphenyl)porphyrins-Zn(II), achieving maximum J_{sc} and V_{oc} measurements of 9.04 mA/cm^2 and 0.57 V, respectively, and maximum power density of 5.2 x 10^3 mW/cm^2.[60] This is similar to what was achieved with a TiO_2 solar cell sensitized with 5-(*p*-carboxyphenylethynyl)-15-(*p*-*N*,*N*-dimethylaminophenylethynyl)-10, 20-bis-(3, 5-di-*tert*-butylphenyl)porphyrin-Zn(II), which resulted with a maximum power density of 4.7 x 10^3 mW/cm^2 (V_{oc} = 0.46 V, J_{sc} = 10.3 mA/cm^2).[61] The cell was then assembled using a ruthenium based dye, N719, which is a derivative of N3, the "gold-standard" dye Grätzel used to achieve conversion efficiencies over 10%.[26,30,61,65,66] The N719-based DSSC was able to achieve a power density of 7.8 x 10^3 mW/cm^2 (V_{oc} = 0.56 V, J_{sc} = 14 mA/cm^2).[61] The DSSCs assembled and tested in this study were found to have greatly diminished performances compared to values sampled from literature, even

when standard deviations were taken into account. The large standard deviations indicate that reproducibility issues were met when assembling these cells.

The power densities stated above are quite typical for porphyrin sensitizers.[26,64] Despite exhibiting promising properties, such as long singlet state lifetimes, strong absorbance in the red and near-IR regions and relative ease to synthesize, porphyrin-based solar cells tend to produce lower open circuit voltages (V_{oc}) compared to ruthenium-based systems.[26,63] This has been commonly attributed to higher rates of intersystem crossing, limiting the number of electrons available in the first excited singlet state, which is where charge injection occurs from.[67] It should be noted that majority of research into the porphyrin as a sensitizer has focused on the role of the singlet state in photochemical events within the solar cell. As a result, the ease of the porphyrin to enter into an excited triplet state has been overlooked and viewed as a hindrance, rather than being explored further. For this reason, investigation of the higher excited states, such as the triplet and S_2 states, needs more focus to improve performance of porphyrin-based systems.

Overall, reproducibility of the *I-V* curves for each porphyrin was difficult to obtain due to many factors: TiO_2 framework, TiO_2 thickness, dye loading, dye aggregation within the framework, and interfacial contact within the photovoltaic device.[1,19,26,51-53,62] This is reflected largely in the variations observed in the photovoltaic properties reported in Tables 4.1, and the standard deviation of average cell power density listed in Table 4.2. Film thickness and morphology were very difficult to replicate, and optimization of these parameters was not the focus of this project. Rather, these measurements were carried out merely to determine if a workable photovoltaic cell was possible to assemble.

It was unclear whether electron injection occurred from the porphyrin S_1 or S_2 state, so the role of TTA in these measurements was unknown. It is also important to note that the power intensity of the Nd:YAG source used for excitation to measure the upconverted S_2 emissions (Chapter 3) is far greater than that of the halogen lamp used to gather the *I-V* curves. The halogen lamp simply may not have supplied the necessary energy for upconversion. ZnTCPP had the strongest S_1 emission of the substituted porphyrins, with decreasing emission intensity of ZnTCPP>>ZnTSPP>ZnTAPP. This same trend is observed with the maximum current densities achieved as shown in Figure 4.3, and power densities reported in Table 4.2. However, ZnTPP was observed to have a much stronger S_1 emission band than the functionalized derivatives, yet has the second weakest current density. This is largely due to lack of a linker group, which is needed to assist efficient electron injection into the semiconductor conduction band.[26] For this reason, it was expected that anionic linker groups would adsorb more strongly onto the titania, improving electron transfer to the semiconductor. It has been found that π conjugation stabilizes the dye, improving electron injection.[26,29,67] ZnTSPP had the strongest S_2 emission band, with decreasing emission intensities observed as ZnTSPP>ZnTCPP>ZnTPP=ZnTAPP, and the second highest cell power density. Further exploration into the role of TTA in the photochemical events in the cell is needed.

4.4 Conclusion

To further evaluate the effects of various porphyrin substituents adsorbed onto mesoporous titania thin films, photovoltaic properties were collected from the corresponding porphyrin-sensitized solar cells. Average power densities collected from the cells were determined to exhibit the following trend: ZnTCPP > ZnTSPP > ZnTPP > ZnTAPP. Photovoltaic performance was largely influenced by the linker groups, which may be due to the

electron injection ability through the ligands. Although the *I-V* curves collected were not impressive by literature standards, the purpose of performing these measurements was to determine whether constructing a working photovoltaic device was possible.

Chapter 5: Conclusion and Future Work

ZnTPP and its functionalized derivatives were studied in this work to determine their photophysical properties on TiO_2 through the use of steady-state absorption and emission measurements. The main objective was to study the TTA capabilities of these sensitizers when adsorbed onto the semiconductor surface. Upconversion via TTA on semiconductor surfaces may prove to be very beneficial for application in DSSCs, where it could be used to improve the spectral response range and conversion efficiency of these photovoltaic devices. Although reproducibility issues were met when measuring upconverted fluorescence, the initial results collected were quite positive indicating that TTA in a semiconductor framework is possible. The detection of upconverted fluorescence with these porphyrin and TiO_2 systems is novel, and further investigation is suggested.

The application of these porphyrins as sensitizers in DSSCs was investigated briefly with the assembly of simple photovoltaic cells. Collection of current and voltage measurements for *I-V* curves indicated that reproducibility was yet another obstacle in producing quality data. However, the assembly of efficient and optimized DSSCs was not the focus of this work. Rather, these measurements were very useful in illustrating the difficulties in synthesizing consistent semiconductor films, in terms of porosity, thickness, impurities, and defects within the framework. Because of the semiconductor's role in charge injection and transport, choice of semiconductor and quality of the film are factors that influence DSSC performance.[26,33] Furthermore, the light source and method of data collection are also important factors that impact data quality. Despite porphyrins being reported as reasonable sensitizers in literature, the above noted factors made it difficult to determine how these porphyrins affected DSSC performance.[26]

Differences between measurements of solution- and titania-based samples indicated the affect that adsorption had on aggregation, a property which is desirable for enhancing TTA, providing an orientation and distance between molecules that facilitate this process. Results collected for the TiO_2-based porphyrin systems indicated formation of H-aggregates, which is favorable for improved TTA efficiency. It is unclear whether the porphyrins self-assembled solely as H-aggregates or a mixture of H- and J-aggregates. This was not investigated in this work, but to improve TTA efficiency it is something that should also be addressed. Porphyrins that are able to accommodate central linking groups would allow more control over aggregation. It is important that conjugated linking groups are used as these will facilitate electron mobility. Additionally, porphyrins with different binding groups should be investigated, particularly with increased conjugation using carboxyl groups. Elongating the distance between the porphyrin and binding group may allow more porphyrins to bind to the semiconductor, increasing the surface concentration.

The semiconductor introduces more variables to these measurements, but is an essential component in optimizing dye-sensitized photovoltaics. This was particularly important when the upconverted fluorescence measurements were conducted, and a significant decrease in emission intensity was observed. The location of the conduction band relative to the S_2 energy level of the porphyrins may be responsible for the low intensity S_2 emission detected. If electron injection occurs readily, these electrons would no longer populate the excited states, leaving the porphyrin unable to fluoresce. Alternatively, charge injection may be occurring readily from the S_1 state, limiting the electrons that are available to undergo intersystem crossing to the T_1 state.[26,67] Population of the triplet state is required for TTA to occur, and a low population of the triplet state drastically impacts population of the S_2 state.[4]

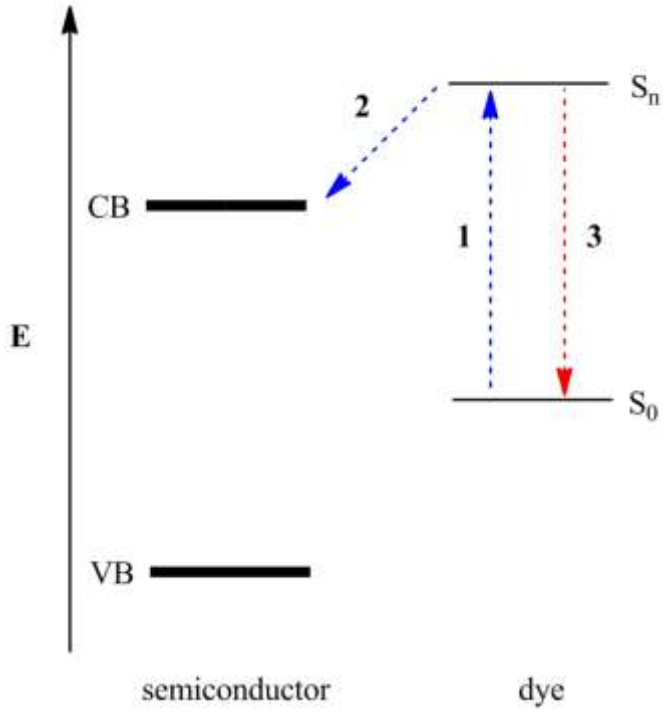

Figure 5.1 Simple energy diagram illustrating some of the electron transfer processes that occur in a DSSC. The following processes are illustrated: (**1**) excitation of the dye, (**2**) charge injection into the conduction band (CB) of the semiconductor, and (**3**) decay of the dye's excited state (which in this case, would be radiative), where S_0 is the ground state of the dye, S_n is an excited state (where n = 1 or 2), VB is valence band of the semiconductor, and E is energy level.

To confirm that TTA is indeed possible and that it occurs with significant emission intensity, measurements should be repeated with a semiconductor whose conduction band is higher in energy than the porphyrin S_2 energy band. Other typical semiconductors used in photovoltaics are ZnO and SnO_2, both of which have larger band gaps than TiO_2 and have demonstrated slower electron injection and mobility in literature.[26] Use of semiconductors with

larger band gaps should make it possible to measure a stronger S_2 emission signal, and may aide in developing a better understanding of the role that the S_2 state serves in charge injection into the semiconductor.

References

(1) Grätzel, M. *Accounts of Chemical Research* **2009**, *42*, 1788-98.

(2) Lakowicz, J. R. *Principles of Fluorescence Spectroscopy*; 2nd ed.; Kluwer Academic/Plenum Publishers: New York, 1999.

(3) Sugunan, S. K. T., U.; Brunet, S. M. K.; Paige, M. F.; Steer, R. P. *J. Phys. Chem. A* **2009**, *113*, 8548-56.

(4) O'Brien, J. A.; Rallabandi, S.; Tripathy, U.; Paige, M. F.; Steer, R. P. *Chemical Physics Letters* **2009**, *475*, 220-2.

(5) O'Brien, J. A. L., Y.; Hooley, E. N.; Ghiggino, K. P.; Steer, R. P.; Paige, M. F. *Can. J. Chem.* **2011**, *89*, 122-9.

(6) Baluschev, S. Y., F.; Miteva, T.; Ahl, S.; Yasuda, A.; Nelles, G.; Knoll, W.; Wegner, G. *Nano Letters* **2005**, *5*, 2482-4.

(7) Auckett, J. E.; Chen, Y. Y.; Khoury, T.; Clady, R. G. C. R.; Ekins-Daukes, N. J.; Crossley, M. J.; Schmidt, T. W. *Journal of Physics: Conference Series* **2009**, *185*, No pp. given.

(8) Singh-Rachford, T. N.; Castellano, F. N. *Coordination Chemistry Reviews* **2010**, *254*, 2560-73.

(9) Steer, R. P. *Journal of Applied Physics* **2007**, *102*.

(10) In *American Chemical Society Symposium*; Gouterman, M., Rentzepis, P. M., Straub, K. D., Eds.; American Chemical Society: Little Rock, Arkansas, 1985.

(11) Kiba, T.; Suzuki, H.; Hosokawa, K.; Kobayashi, H.; Baba, S.; Kakuchi, T.; Sato, S. *Journal of Physical Chemistry B* **2009**, *113*, 11560-3.

(12) Li, X. Q.; Zhang, L.; Mu, J. *Colloids and Surfaces A-Physicochemical and Engineering Aspects* **2007**, *311*, 187-90.

(13) Scolaro, L. M.; Romeo, A.; Castriciano, M. A.; Micali, N. *Chemical Communications* **2005**, 3018-20.

(14) Milgrom, L. R. *The Colours of Life: An Introduction to the Chemistry of Porphyrins and Related Compounds*; Oxford University Press Inc.: New York, 1997.

(15) *The Porphyrin Handbook*; Kadish, K. M. S., K. M.; Guilard, R., Ed.; Academic Press: San Diego, 2000; Vol. 16.

(16) Ning, Z. J.; Fu, Y.; Tian, H. *Energy & Environmental Science* **2010**, *3*, 1170-81.

(17) Martinez-Diaz, M. V.; de la Torrea, G.; Torres, T. *Chemical Communications* **2010**, *46*, 7090-108.

(18) Wagner, K.; Griffith, M. J.; James, M.; Mozer, A. J.; Wagner, P.; Triani, G.; Officer, D. L.; Wallace, G. G. *Journal of Physical Chemistry C* **2011**, *115*, 317-26.

(19) Lo, C. F.; Hsu, S. J.; Wang, C. L.; Cheng, Y. H.; Lu, H. P.; Diau, E. W. G.; Lin, C. Y. *Journal of Physical Chemistry C* **2010**, *114*, 12018-23.

(20) Grätzel, M. *Philosophical Transactions of The Royal Society A* **2007**, *365*, 993-1005.

(21) Bessho, T.; Zakeeruddin, S. M.; Yeh, C. Y.; Diau, E. W. G.; Grätzel, M. *Angewandte Chemie-International Edition* **2010**, *49*, 6646-9.

(22) Gajjela, S. R.; Ananthanarayanan, K.; Yap, C.; Grätzel, M.; Balaya, P. *Energy & Environmental Science* **2010**, *3*, 838-45.

(23) Gentilini, D.; D'Ercole, D.; Gagliardi, A.; Brunetti, A.; Reale, A.; Brown, T.; Di Carlo, A. *Superlattices and Microstructures* **2010**, *47*, 192-6.

(24) Reijnders, L. *Journal of Cleaner Production* **2010**, *18*, 307-12.

(25) Lee, C. Y.; Hupp, J. T. *Langmuir* **2009**, *26*, 3760-5.

(26) Hagfeldt, A.; Boschloo, G.; Sun, L.; Kloo, L.; Pettersson, H. *Chemical Reviews* **2010**, *110*, 6595-663.

(27) Grätzel, M. *Nature* **2001**, *414*, 338-44.

(28) Jayaweera, P. V. V.; Perera, A. G. U.; Tennakone, K. *Inorganica Chimica Acta* **2008**, *361*, 707-11.

(29) Dos Santos, T.; Morandeira, A.; Koops, S.; Mozer, A. J.; Tsekouras, G.; Dong, Y.; Wagner, P.; Wallace, G.; Earles, J. C.; Gordon, K. C.; Officer, D.; Durrant, J. R. *Journal of Physical Chemistry C* **2010**, *114*, 3276-9.

(30) Katoh, R. F., A.; Yoshihara, T.; Hara, K.; Fujihashi, G.; Takano, S.; Murata, S.; Arakawa, H.; Tachiya, M. *J. Phys. Chem. B* **2004**, *108*, 4818-22.

(31) Sun, Y. O., A. C.; Myahkostupov, M.; Castellano, F. N. *Acs Applied Materials & Interfaces* **2010**, *2*, 2039-45.

(32) Zukalova, M.; Prochazka, J.; Zukal, A.; Yum, J. H.; Kavan, L. *Inorganica Chimica Acta* **2008**, *361*, 656-62.

(33) Agarwala, S.; Ho, G. W. *Materials Letters* **2009**, *63*, 1624-7.

(34) Choi, S. Y.; Mamak, M.; Coombs, N.; Chopra, N.; Ozin, G. A. *Advanced Functional Materials* **2004**, *14*, 335-44.

(35) Chen, D. H., F.; Cheng, Y. B.; Caruso, R. A. *Adv. Mater.* **2009**, *21*, 2206-10.

(36) Robertson, N. *Angewandte Chemie-International Edition* **2006**, *45*, 2338-45.

(37) Liu, X.; Tripathy, U.; Bhosale, S. V.; Langford, S. J.; Steer, R. P. *Journal of Physical Chemistry A* **2008**, *112*, 8986-98.

(38) Rochford, J.; Galoppini, E. *Langmuir* **2008**, *24*, 5366-74.

(39) Kira, A.; Matsubara, Y.; Iijima, H.; Umeyama, T.; Matano, Y.; Ito, S.; Niemi, M.; Tkachenko, N. V.; Lemmetyinen, H.; Imahori, H. *Journal of Physical Chemistry C* **2010**, *114*, 11293-304.

(40) Friesen, B. A.; Rich, C. C.; Mazur, U.; McHale, J. L. *Journal of Physical Chemistry C* **2010**, *114*, 16357-66.

(41) Rochford, J.; Chu, D.; Hagfeldt, A.; Galoppini, E. *Journal of the American Chemical Society* **2007**, *129*, 4655-65.

(42) Biswas, S.; Ahn, H.-Y.; Bondar, M. V.; Belfield, K. D. *Langmuir* **2012**, *28*, 1515-22.

(43) Cherian, S.; Wamser, C. C. *Journal of Physical Chemistry B* **2000**, *104*, 3624-9.

(44) Danger, B. R.; Bedient, K.; Maiti, M.; Burgess, I. J.; Steer, R. P. *Journal of Physical Chemistry A* **2010**, *114*, 10960-8.

(45) Araghi, M. M., V.; Moghadam, M.; Tangestaninejad, S.; Mohammdpoor-Baltork, I. *Dalton Transactions* **2012**, *41*, 11745-52.

(46) Neta, P. *Journal of Physical Chemistry* **1981**, *86*, 3678-84.

(47) Kalyanasundaram, K.; Neumann-Spallart, M. *Journal of Physical Chemistry* **1982**, *86*, 5163-69.

(48) Szmytkowski, J.; Brunet, S. M. K.; Tripathy, U.; O'Brien, J. A.; Paige, M. F.; Steer, R. P. *Chemical Physics Letters* **2011**, *501*, 278-82.

(49) Misawa, K.; Kobayashi, T. *The Journal of Chemical Physics* **1999**, *110*, 5844-50.

(50) Agarwala, S.; Kevin, M.; Wong, A. S. W.; Peh, C. K. N.; Thavasi, V.; Ho, G. W. *ACS Applied Materials & Interfaces* **2010**, *2*, 1844-50.

(51) Zhang, Y.; Xie, Z. B.; Wang, J. *Nanotechnology* **2009**, *20*, 505602.

(52) Zhang, Y.; Xie, Z. B.; Wang, J. *ACS Applied Materials & Interfaces* **2009**, *1*, 2789-95.

(53) Yang, W. G.; Wan, F. R.; Chen, Q. W.; Li, J. J.; Xu, D. S. *Journal of Materials Chemistry* **2010**, *20*, 2870-6.

(54) Yun, H. J. L., H.; Joo, J. B.; Kim, N. D.; Yi, J. *Electrochemistry Communications* **2010**, *12*, 769-72.

(55) Hoang, S. G., S.; Hahn, N. T.; Bard, A. J.; Mullins, C. B. *Nano Letters* **2012**, *12*, 26-32.

(56) Schwenzer, B. W., L.; Swensen, J. S.; Padmaperuma, A. B.; Silverman, G.; Korotkov, R.; Gaspar, D. J. *Langmuir* **2012**, *28*, 10072-81.

(57) Fanis, L. *Nanocrystalline Solar Cell Kit: Recreating Photosynthesis*; 2nd ed.; ICE Publication: Madison, 2008.

(58) Kron, G.; Rau, U.; Werner, J. H. *Journal of Physical Chemistry B* **2003**, *107*, 13258-61.

(59) Wang, Y.; Wang, X.; Ghosh, S. K.; Lu, H. P. *Journal of the American Chemical Society* **2009**, *131*, 1479-87.

(60) Seo, K. D. L., M. J.; Song, H. M.; Kang, H. S.; Kim, H. K. *Elsevier* **2012**, *94*, 143-9.

(61) Biroli, A. O. T., F.; Pizzotti, M.; Biaggi, C.; Ugo, R.; Caramori, S.; Aliprandi, A.; Bignozzi, C. A.; De Angelis, F.; Giorgi, G.; Licandro, E.; Longhi, E. *J. Phys. Chem. C* **2011**, *115*, 23170-82.

(62) Wang, Q.; Carnpbell, W. M.; Bonfantani, E. E.; Jolley, K. W.; Officer, D. L.; Walsh, P. J.; Gordon, K.; Humphry-Baker, R.; Nazeeruddin, M. K.; Gratzel, M. *Journal of Physical Chemistry B* **2005**, *109*, 15397-409.

(63) Mozer, A. J. W., P.; Officer, D. L.; Wallace, G. G.; Campbell, W. M.; Miyashita, M.; Sunahara, K.; Mori, S. *Chemical Communications* **2008**, 4741-3.

(64) Li, L. L. D., E. W. G. *Chem. Soc. Rev.* **2013**, *42*, 291-304.

(65) Lee, C.-W.; Lu, H.-P.; Lan, C.-M.; Huang, Y.-L.; Liang, Y.-R.; Yen, W.-N.; Liu, Y.-C.; Lin, Y.-S.; Diau, E. W.-G.; Yeh, C.-Y. *Chemistry – A European Journal* **2009**, *15*, 1403-12.

(66) Uzaki, K.; Nishimura, T.; Usagawa, J.; Hayase, S.; Kono, M.; Yamaguchi, Y. *Journal of Solar Energy Engineering-Transactions of the ASME* **2010**, *132*.

(67) Monteiro, C. J. P. P., J.; Pereira, M. M.; Arnaut, L. G. *Photochem. Photobiol. Sci.* **2012**, *11*, 1233-8.